

Semi-Blind Receivers for Hybrid Reflecting and Sensing RIS

Amarilton L. Magalhães, *Graduate Student Member, IEEE* and André L. F. de Almeida, *Senior Member, IEEE*

Abstract—Recent research has delved into advanced designs for reconfigurable intelligent surfaces (RIS) with integrated sensing functions. One promising concept is the hybrid RIS (HRIS), which blends sensing and reflecting meta-atoms. This enables HRIS to process signals, aiding in channel estimation (CE) and symbol detection tasks. This paper formulates semi-blind receivers for HRIS-aided wireless communications that enable joint symbol and CE at the HRIS and BS. The proposed receivers rely on a new tensor modeling approach for the signals received at both the HRIS and BS while exploiting a tensor signal coding scheme at the transmit side. Specifically, by capitalizing on the multilinear structures of the received signals, we develop iterative and closed-form receiver algorithms for joint estimation of the uplink channels and symbols at both the HRIS and the BS. Enabling joint channel and symbol estimation functionalities, the proposed receivers offer symbol decoding capabilities to the HRIS and ensure ambiguity-free separate CE without requiring an *a priori* training stage. We also study identifiability conditions ensuring a unique joint channel and symbol recovery and discuss the computational complexities and tradeoffs involved by the proposed semi-blind receivers. Our findings demonstrate the competitive performances of the proposed algorithms at the HRIS and the BS and uncover distinct performance trends based on the possible combinations of HRIS-BS receiver pairs. Finally, extensive numerical results elucidate the interplay between power splitting, symbol recovery, and CE accuracy in HRIS-assisted communications. Such insights are pivotal for optimizing receiver design and enhancing system performance in future HRIS deployments.

Index Terms—Reconfigurable surfaces, hybrid RIS, semi-blind receivers, joint channel and symbol estimation, tensor modeling.

I. INTRODUCTION

RECENTLY, reconfigurable intelligent surface (RIS) has been envisioned as a key enabling technology for deploying future wireless networks, for example, the sixth generation (6G) [1]–[4]. RIS is a large array of passive reflecting elements mounted on a planar surface that can independently interact with the impinging electromagnetic waves by means of software-controllable phase shifts [1], [2], [5], [6]. Several applications for RIS can be found in the literature, such as coverage for users located in dead zones and co-channel interference suppression for users located at the edges of cells [6], [7], improvement of the physical layer security [8], integration with unmanned aerial vehicles (UAVs) and other aerial platforms [9], simultaneous wireless information

and power transfer (SWIPT) [6], and integrated sensing and communications (ISAC) [10], to mention a few.

In this context, accurate channel state information (CSI) is crucial in optimizing RIS-assisted systems [11], [12]. Its acquisition is necessary and challenging for designing the RIS reflection coefficients as well as the precoder/beamformer at both the base station (BS) and user terminal (UT) [7], [13]–[15]. In general, channel estimation (CE) in multiple-input multiple-output (MIMO) RIS-assisted wireless communication systems faces two main challenges. The first is related to a notable increase in the required number of pilots compared to conventional systems, driven by a large number of RIS elements, leading to a significantly large number of channel coefficients [16]–[21]. The second one is the unavailability of estimating the separate channels from the RIS-assisted one, namely UT-RIS and RIS-BS links, since the passive RIS (PRIS) acts only as signal reflector [17], [19]–[22] and only the cascaded channel is estimated¹ so that all the receiver processing is done only at the BS or the UT. Solutions in the literature that have addressed these challenges are usually sorted into two families of methods: the first one incorporates novel algorithms to leverage the channel structure while preserving the original hardware properties of the PRIS, while the second one involves modifying its hardware architecture to allow for additional signal processing capabilities at the RIS [16]. This paper relies on the second approach.

Given the passive nature of the RIS, most CE-related work commonly falls into cascaded CE, which is sufficient for applications like rate maximization and beamforming design. In contrast, a scaling ambiguity-free separate CE is preferred for applications like channel sounding, user localization, and mobility tracking, as highlighted in [25]. For instance, in mobility scenarios, [26] argues that separate CE facilitates channel tracking by identifying the behavior of the individual links under temporal variations. As pointed out therein, cascaded CE complicates tracking as changes occur in either the UT-RIS, RIS-BS, or both links. Moreover, in scenarios where the UT-RIS channel changes more rapidly than the RIS-BS one, the former must be estimated more often, while the latter not, highlighting the importance of recovering such channels individually instead of the combined one [13], [27]. On the other hand, some designs depend on the availability of the individual channels, such as in [28], [29], and [30]. The

This work is partially supported by the National Institute of Science and Technology (INCT-Signals), sponsored by Brazil's National Council for Scientific and Technological Development (CNPq) under grant 406517/2022-3, and CAPES/Brazil. A. L. F. de Almeida is partially supported by CNPq under grant 312491/2020-4.

¹The cascaded (RIS-assisted, concatenated, composite, combined, or compound) channel comprises the joint effect of both UT-RIS and RIS-BS channels. Sometimes, the cascaded CE is made through its decoupled version, whose estimated matrices are affected by scaling ambiguities, as shown in [23] and [24]. This necessitates complementary techniques to acquire the knowledge required for scaling removal.

importance of estimating the involved channels separately is reinforced in [19], [31]–[34].

From a hardware perspective, a notable study was carried out in [35]. Specifically, the authors in [35] proposed a RIS structure by sparsely replacing some passive reflecting elements with active sensors connected to a single receive RF chain² each, thereby enabling baseband processing at the RIS controller. These active elements merely sense the impinging signal without reflection. Adopting this hybrid architecture³, the authors introduced a CE scheme based on compressed sensing and deep learning, achieving minimal pilot overhead while facilitating the CE process at the sacrifice of increased hardware complexity and power consumption. Inspired by the pioneering research in [35], such a hybrid architecture has been comprehensively investigated in subsequent works, such as in [20]–[22], [34] and references therein.

In contrast to RIS, another metasurface-based technology called dynamic metasurface antenna (DMA) has emerged to enable low-cost, extremely large antenna arrays [37]. Despite the differences between the RIS and DMA operation, it is attainable to envision a hybrid meta-atom capable of reflecting and sensing since their meta-atoms share similarities [1]. Motivated by DMAs, a novel metasurface was introduced in [38], where the physical structure of each meta-atom is modified to couple small portions of the incoming wave. Relying on this paradigm, [1] introduced the co-called hybrid RIS (HRIS) architecture, outlining its prospects/obstacles. These meta-atoms are integrated into sampling waveguides similarly to [38], and the sensed signals are forwarded *via* analog combining to F chains, whose outputs enable signal processing in the digital domain while retaining its reconfigurable reflection functionalities. The relationship of both reflected and sensed portions is dictated by the coupling level, controlled by changing either the substrate-integrated waveguide or the annular slot sizes [1]. Based on this architecture and leveraging transmitted pilots, the work [19] exploits the signal processing capabilities at the HRIS to estimate the UTs-HRIS channels from the sensed signal part, while the HRIS-BS channel is estimated at the BS from the reflected one. This is accomplished by exploiting a feedback control link (CL)⁴ between the HRIS and the BS, through which the BS acquires the UT-HRIS channel matrix estimated at the HRIS. A detailed study of different hybrid architectures is provided in [2].

Tensor decompositions have been successfully applied to model wireless communication systems [39], [40], including blind/semi-blind receivers [41], space-time (ST)/space-time-frequency (STF) coding schemes, [42], [43]. These works have highlighted the effectiveness of tensor decompositions and their powerful uniqueness properties to harness the multidimensional nature of received signals and channels for deriving receiver algorithms capable of operating semi-blindly

under less restrictive requirements than competing (matrix-based) methods while offering good performance/complexity tradeoffs. See [44]–[47] and references therein for an overview. Recent works have introduced tensor modeling to the context of passive RIS (PRIS)-aided communications to solve problems such as CE, semi-blind joint CE and symbol detection, and channel tracking [23], [24], [48]–[51]. Among these works, parallel factor (PARAFAC) decomposition, also known as canonical polyadic decomposition (CPD) [52] was applied to solve the CE estimation problem in a PRIS approach [23], [24], [53], while [21] in a hybrid semi-passive one. More recently, [51] proposed PARAFAC-based algorithms for CE accounting for RIS operating under imperfections from real-world effects. In particular, without requiring prior CE via training sequences, [49] and [50] introduced data-aided semi-blind CE (SBCE) methods for PRIS-aided communications using Khatri-Rao ST coding (KRSTC), integrating symbol detection and CE through closed-form and iterative receivers, respectively. In [50], the authors exploited the PARATUCK tensor decomposition [54], [55], while a generalized version was presented in [49]. Nonetheless, KRSTC thresholds the number of streams to that of transmitting antennas.

Different from the aforementioned works, in most restricted to PRIS, where the cascaded CE problem is concentrated at the BS, this paper shows that the estimation of the individual channels and the transmitted symbols can be achieved jointly at both the HRIS and BS in a semi-blind fashion by resorting to tensor modeling. Moreover, in contrast to [19], which relies on pilot-assisted CE at the HRIS, our approach expands upon this by incorporating joint symbol and CE directly at the HRIS. This is achieved iteratively or in closed form using simple algorithms without the need for pilot training. As will be discussed later, empowering HRIS with symbol-decoding capabilities can be useful in a number of scenarios.

The contributions of this paper are summarized as follows:

First, leveraging the HRIS architecture [1] and assuming a one-way structured time domain protocol, we formulate the received signals at both the HRIS and BS using a new tensor formalism that disentangles the received signal into effective channel tensors and coded signal tensors following PARAFAC and/or Tucker decompositions. Exploiting these tensor models allows the HRIS to jointly estimate the associated channel and decode the transmitted symbols in a semi-blind fashion. By transmitting data symbols in advance during the CE stage, our approach can improve data rate and reduce symbol decoding delay compared to pilot-only methods.

Second, capitalizing on the proposed tensor models, we derive semi-blind joint symbol and CE methods for HRIS-aided MIMO wireless communication systems. More specifically, we formulate iterative and closed-form receiver pairs that are split between HRIS and BS to efficiently solve the SBCE problem. The proposed receivers eliminate the need for training sequences and additional steps for scaling ambiguity removal on the estimated channels and symbols, while partially circumventing the path-loss effects induced by the cumulated UT-HRIS and HRIS-BS links.

Third, we study identifiability at both the HRIS and the BS, derive a set of conditions that ensure a unique channel and

²This receive RF chain is comprised of a low noise amplifier, a downconverter mixer (from RF to baseband), and an analog-to-digital converter [36].

³This architecture has been referred to in the literature using different terminologies, such as *hybrid semi/passive* RIS, *sensing* RIS, *receiving* RIS, or simply *hybrid* RIS. Such an architecture should not be confused with the one considered in this paper, as will be clear later.

⁴This CL is used to reconfigure the reflection patterns of the RIS. In [19], error-free transmission over a high throughput CL was considered.

symbol recovery, and discuss the computational complexities and trade-offs involved by the proposed semi-blind receivers.

Finally, extensive numerical results showcase the interplay between power splitting, symbol recovery, and CE accuracy in HRIS-assisted communications. Our findings demonstrate competitive performances among receivers at the HRIS and BS and uncover distinct performance trends based on the combinations of HRIS-BS receiver pairs. We also delve into a brief exploration of scenarios where a joint symbol and CE at the HRIS are useful.

The rest of the paper is organized as follows. Section II describes the system and signal models at the HRIS and the BS, including the transmission protocol and the main assumptions. Section III derives the corresponding tensor signal models and develops the core equations associated with the receiver design. The proposed semi-blind receivers for the HRIS and the BS are detailed, respectively, in Sections IV and V. Section VI discusses identifiability, uniqueness, and computational complexity. Section VII contains our numerical results, while Section VIII provides a discussion on potential use cases benefiting from the proposed joint channel/symbol estimation at the HRIS. Conclusions are drawn in Section IX.

A. Notation and properties

We utilize lowercase a , bold lowercase \mathbf{a} , bold uppercase \mathbf{A} , and calligraphic \mathcal{A} to denote scalars, column vectors, matrices, and tensors, respectively. The (i, j) -th element of \mathbf{A} is denoted as $[\mathbf{A}]_{i,j}$. Transpose, conjugate, and Moore-Penrose pseudo-inverse of \mathbf{A} are denoted as \mathbf{A}^T , \mathbf{A}^* , and \mathbf{A}^\dagger , respectively. The operator $\text{diag}\{\mathbf{a}\}$ constructs a diagonal matrix from \mathbf{a} . $\lceil a \rceil$ is the smallest integer greater than or equal to a , and the Frobenius norm is indicated by $\|\cdot\|_F$. The symbols \diamond , and \otimes represent the Khatri-Rao and Kronecker matrix products, respectively. Stated $\mathbf{A} \in \mathbb{C}^{I \times J}$, the vectorization operator, denoted as $\text{vec}\{\mathbf{A}\}$, yields the vector $\mathbf{a} \in \mathbb{C}^{JI \times 1}$. Conversely, the reverse operation, $\text{unvec}_{I \times J}(\mathbf{a})$, restores the matrix \mathbf{A} . A tensor $\mathcal{A} \in \mathbb{C}^{I_1 \times I_2 \times \dots \times I_P}$ is a multidimensional array with order P , and unfolding is the procedure that reshapes it into a matrix; for instance, $[\mathcal{A}]_{(1)} \in \mathbb{C}^{I_1 \times I_3 I_2}$, $[\mathcal{A}]_{(2)} \in \mathbb{C}^{I_2 \times I_3 I_1}$ and $[\mathcal{A}]_{(3)} \in \mathbb{C}^{I_3 \times I_2 I_1}$ denote the wide 1-mode, 2-mode, and 3-mode unfoldings of a third-order tensor $\mathcal{X} \in \mathbb{C}^{I_1 \times I_2 \times I_3}$. In addition, $\mathcal{I}_{3,P} \in \mathbb{R}^{P \times P \times P}$ is the 3rd-order identity tensor. Consider two P -th order tensors $\mathcal{A} \in \mathbb{C}^{I_1 \times \dots \times I_P \times \dots \times I_P}$ and $\mathcal{B} \in \mathbb{C}^{J_1 \times \dots \times J_q \times \dots \times J_P}$, such that $I_P = J_P$ and $I_p = J_q$. We define the *mode-wise contraction* operation as a contraction between slices of \mathcal{A} and \mathcal{B} . For simplicity, we assume this operation affects the P -mode of such tensors, which gives

$$\mathcal{A} \circledast_p^q \mathcal{B} \doteq \mathcal{C} \in \mathbb{C}^{I_1 \times \dots \times I_{p-1} \times I_{p+1} \times \dots \times I_{p-1} \times J_1 \times \dots \times J_{q-1} \times J_{q+1} \times \dots \times J_P}, \quad (1)$$

where the P -mode slice of the $(2P-3)$ -th order tensor \mathcal{C} results from the tensor contraction between the P -mode slices of \mathcal{A} and \mathcal{B} , involving mode p of \mathcal{A} and mode q of \mathcal{B} . For instance, the mode-wise contraction of two 3rd-order tensors \mathcal{A} and \mathcal{B} is accomplished by

$$\mathcal{C}_{..j} = (\mathcal{A} \circledast_p^q \mathcal{B})_{..j} = \mathcal{A}_{..j} \circledast_p^q \mathcal{B}_{..j}, \quad j = 1, \dots, J_P. \quad (2)$$

Throughout this paper, we make use of the following identities:

$$\text{vec}\{\mathbf{ABC}\} = (\mathbf{C}^T \otimes \mathbf{A})\text{vec}\{\mathbf{B}\}. \quad (3)$$

$$\mathbf{AB} \otimes \mathbf{CD} = (\mathbf{A} \otimes \mathbf{C})(\mathbf{B} \otimes \mathbf{D}). \quad (4)$$

$$\text{diag}\{\mathbf{a}\} \mathbf{b} = \text{diag}\{\mathbf{b}\} \mathbf{a}, \quad \text{for } \mathbf{a}, \mathbf{b} \in \mathbb{C}^{P \times 1}. \quad (5)$$

We consider a single-user HRIS-assisted MIMO communication system where the multi-antenna UT and BS are equipped with L and M antennas, respectively. This work considers uplink communication⁵. We suppose there is no direct link between the BS and UT due to blockages, and it is left out of the signal model. Hence, only non-LoS (NLoS) transmission is considered. In addition, the HRIS controller is linked to the BS *via* CL, which is assumed to be error-free. The UT communicates with the BS through the assistance of an HRIS comprising a metasurface of N meta-atom elements connected *via* analog combining to a digital controller through N_c RF chains [1], [19], as depicted in Fig. 1. We use the power split parameter $\rho_n(t)$ to represent the fraction of the signal reflected from the n -th HRIS meta-atom at the t -th time instant. Hence, $1 - \rho_n(t)$ denotes the sensed portion forwarded to the RF chains. $e^{j\psi_n(t)}$ is the controllable reflecting phase-shift of the n -th meta-atom at the t -th time instant, and $e^{j\phi_{n_c,n}(t)}$ is the phase-shift that models the joint effect on the wave captured by the n -th meta-atom element at the t -th time instant caused by the adjustable frequency response of the meta-material element by phase-shifting and the propagation inside the waveguide, which forwards to the n_c -th RF chain. We consider $\psi_n(t)$, $\phi_{n_c,n}(t) \in [0, 2\pi)$. A structured two-block time-domain transmission is adopted, during which the semi-blind CE occurs in the first block of T_s symbol periods, comprised of K sub-frames of T symbol periods each (i.e., $T_s = KT$), while the second one has T_d symbol periods dedicated for pure data transmission. Note that during T_s symbol periods, this structure spends the same time as that dedicated to addressing CE in [19], in which only pilots are transmitted. The key difference is that in our approach, data symbols are transmitted in advance during T_s symbol periods, enhancing the data rate and reducing the overall symbol decoding delay. A quasi-static flat-fading channel with coherence time T_c is assumed, where UT-HRIS and HRIS-BS channels remain constant during at least T_s symbol periods, with $T_s \ll T_c$. Digital precoding/combiner design, RIS phase shift optimization, and signal processing in the second block fall outside the scope of this work.

II. SYSTEM AND SIGNAL MODELS

A. Tensor ST coding (TSTC)

Before transmission at the UT, the input symbols undergo a tensor ST coding scheme [42], which incorporates spatial multiplexing with spreading, enabling a linear combination of streams across both spatial and temporal dimensions. Consequently, our transmit signal model extends beyond that exploited in [50]. This way, all the R independent streams at

⁵Although the primary focus of this paper is on uplink communication from the UT to BS, the results obtained can also be applied to downlink communication in the opposite direction by leveraging uplink-downlink channel reciprocity and simply reversing the roles of the transmitter and receiver.

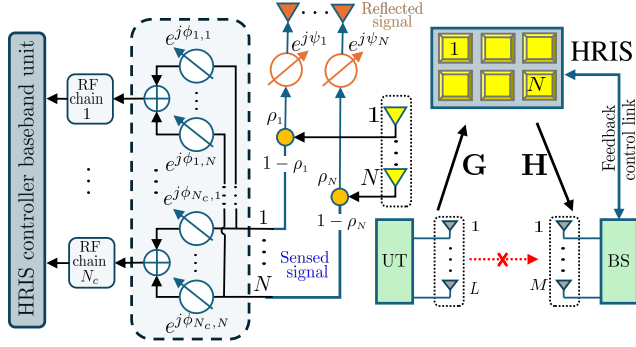


Fig. 1. System model.

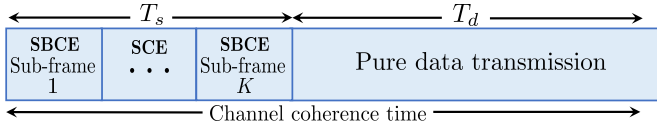


Fig. 2. Transmission time structure.

the t -th symbol period of the k -th sub-frame ($k = 1, \dots, K$) are split across L combiners. At the l -th combiner, each independent symbol $x_{r,t}$ ($r = 1, \dots, R$) is coded by $w_{l,r,k}$ ($l = 1, \dots, L$). After that, the R coded signals are combined to yield $s_{l,t,k} = (1/\sqrt{L}) \sum_{r=1}^R w_{l,r,k} x_{r,t}$, to be forwarded to the l -th transmitting antenna. We assume that coefficients $w_{l,r,t,k}$ remain constant within the k -th sub-frame and may vary from one sub-frame to another, which means $w_{l,r,t,k} = w_{l,r,k}$, for $t = 1, \dots, T$. Collecting the coded symbols forwarded to all L antennas, we have $\mathbf{s}_{t,k} = \mathbf{W}_k \mathbf{x}_t \in \mathbb{C}^{L \times 1}$, in which $\mathbf{x}_t \doteq [x_{1,t}, \dots, x_{R,t}]^T \in \mathbb{C}^{R \times 1}$ is comprised by symbols coming from all the R data streams at the t -th time instant, and $\mathbf{W}_k \in \mathbb{C}^{L \times R}$ is the coding matrix of the k -th sub-frame gathering all R inputs and L outputs, i.e., $[\mathbf{W}_k]_{l,r} = w_{l,r,k}$. The HRIS parameters (ρ , ψ and ϕ) are assumed to be reconfigured just like the coefficients $w_{l,r,k}$, which leads to $\rho_{n,t,k} = \rho_{n,k}$, $\psi_{n,t,k} = \psi_{n,k}$ and $\phi_{n_c,n,t,k} = \phi_{n_c,n,k}$, following [19].

The portion of the signal transmitted by the L UT antennas, sensed by the N HRIS meta-atoms, and then forwarded to the N_c RF-chains via analog combining at the t -th time slot of the k -th sub-frame, is given by $\mathbf{y}_{t,k}^{\text{RC}} = \Phi_k \mathbf{G} \mathbf{W}_k \mathbf{x}_t + \boldsymbol{\nu}_{t,k}^{\text{RC}} \in \mathbb{C}^{N_c \times 1}$, where $\boldsymbol{\nu}_{t,k}^{\text{RC}}$ is the associated additive noise at the HRIS, $\mathbf{G} \in \mathbb{C}^{N_c \times L}$ is the UT-HRIS channel matrix and $\Phi_k \in \mathbb{C}^{N_c \times N}$ is the sensing phase shift matrix of the k -th sub-frame that yields the analog combining carried out by HRIS [19], in which $[\Phi_k]_{n_c,n} = \sqrt{(1-\rho_{n,k})/N_c} e^{j\phi_{n_c,n,k}}$. Meanwhile, the received signal at the BS, corresponding to the portion of the signal reflected by the HRIS, is given by $\mathbf{y}_{t,k}^{\text{BS}} = \mathbf{H} \text{diag}\{\boldsymbol{\psi}_k\} \mathbf{G} \mathbf{W}_k \mathbf{x}_t + \boldsymbol{\nu}_{t,k}^{\text{BS}} \in \mathbb{C}^{M \times 1}$, where $\boldsymbol{\nu}_{t,k}^{\text{BS}}$ represents the noise at the BS, $\mathbf{H} \in \mathbb{C}^{M \times N}$ is the HRIS-BS channel matrix, and $\boldsymbol{\psi}_k \doteq [\sqrt{\rho_{1,k}} e^{j\psi_{1,k}}, \dots, \sqrt{\rho_{N,k}} e^{j\psi_{N,k}}] \in \mathbb{C}^{N \times 1}$ is the reflecting phase-shift beam. After T time slots of the k -th sub-frame, we collect column-wise $\mathbf{y}_{t,k}^{\text{RC}}$ and $\mathbf{y}_{t,k}^{\text{BS}}$ into the matrices $\mathbf{Y}_k^{\text{RC}} \doteq [\mathbf{y}_{1,k}^{\text{RC}}, \dots, \mathbf{y}_{T,k}^{\text{RC}}] \in \mathbb{C}^{N_c \times T}$ and $\mathbf{Y}_k^{\text{BS}} \doteq [\mathbf{y}_{1,k}^{\text{BS}}, \dots, \mathbf{y}_{T,k}^{\text{BS}}] \in \mathbb{C}^{M \times T}$, respectively, to get

$$\mathbf{Y}_k^{\text{RC}} = \Phi_k \mathbf{G} \mathbf{W}_k \mathbf{X} + \mathbf{V}_k^{\text{RC}} \in \mathbb{C}^{N_c \times T} \quad (6)$$

and

$$\mathbf{Y}_k^{\text{BS}} = \mathbf{H} \text{diag}\{\boldsymbol{\psi}_k\} \mathbf{G} \mathbf{W}_k \mathbf{X} + \mathbf{V}_k^{\text{BS}} \in \mathbb{C}^{M \times T}, \quad (7)$$

where $\mathbf{X} = [\mathbf{x}_1, \dots, \mathbf{x}_T] \in \mathbb{C}^{R \times T}$ is the symbol matrix, which collects T symbol periods of the R data streams. Here, \mathbf{V}_k^{RC} and \mathbf{V}_k^{BS} stand for the noise matrices associated with sub-frame k at the HRIS and BS, respectively.

B. Khatri-Rao ST coding (KRSTC)

We also consider KRSTC for comparison purposes. Following [56], [50] and the adopted time protocol, each independent symbol $x_{l,t}$ ($l = 1, \dots, L$) is coded by a coefficient $\lambda_{l,k}$ ($k = 1, \dots, K$) to yield $s_{l,t,k} = \lambda_{l,k} x_{l,t}$, which is then forwarded to the l -th transmitting antenna. Collecting the coded symbols for all L antennas, we have $\mathbf{s}_{t,k} = \text{diag}\{\boldsymbol{\lambda}_k\} \mathbf{x}_t \in \mathbb{C}^{L \times 1}$, in which $\mathbf{x}_t \doteq [x_{1,t}, \dots, x_{L,t}]^T \in \mathbb{C}^{L \times 1}$ and $\boldsymbol{\lambda}_k \doteq [\lambda_{1,k}, \dots, \lambda_{L,k}]^T \in \mathbb{C}^{L \times 1}$ is the coding vector of the k -th sub-frame. In this case, (6) and (7) are, respectively, recast as

$$\mathbf{Y}_k^{\text{RC}} = \Phi_k \mathbf{G} \text{diag}\{\boldsymbol{\lambda}_k\} \mathbf{X} + \mathbf{V}_k^{\text{RC}} \in \mathbb{C}^{N_c \times T}, \quad (8)$$

$$\mathbf{Y}_k^{\text{BS}} = \mathbf{H} \text{diag}\{\boldsymbol{\psi}_k\} \mathbf{G} \text{diag}\{\boldsymbol{\lambda}_k\} \mathbf{X} + \mathbf{V}_k^{\text{BS}} \in \mathbb{C}^{M \times T}, \quad (9)$$

where the symbol matrix is recast as $\mathbf{X} \in \mathbb{C}^{L \times T}$. Note that KRSTC is a special case of TSTC, where the coding matrix associated with the k -th sub-frame is diagonal. This implies $R = L$ and the absence of signal combining/multiplexing at the transmitter. The signal model of (9), which follows the PARATUCK model, was considered in [50] for the PRIS case.

III. TENSOR SIGNAL MODELING

In the following, we recast the received signals using a tensor approach. Indeed, these signals are three-way (3D) arrays having one spatial dimension (N_c for the HRIS or M for the BS) and two temporal dimensions (T and K). These tensor models are exploited later to derive the proposed HRIS-BS semi-blind receiver pairs.

The signal sensed at the HRIS associated with the k -th sub-frame, defined in (6), can be rewritten as $\mathbf{Y}_{\cdot\cdot k}^{\text{RC}} = \Phi_{\cdot\cdot k} \mathbf{G} \mathbf{W}_{\cdot\cdot k} \mathbf{X} + \mathbf{V}_{\cdot\cdot k}^{\text{RC}}$, which can be viewed as a frontal slice of the 3rd-order sensed signal tensor $\mathcal{Y}^{\text{RC}} \in \mathbb{C}^{N_c \times T \times K}$ constructed by concatenating $\mathbf{Y}_{\cdot\cdot k}^{\text{RC}}$ along the third mode, for $k = 1, \dots, K$. For presentation convenience, in the following equations we consider the noiseless part of \mathcal{Y}^{RC} , defined as $\tilde{\mathcal{Y}}^{\text{RC}}$, such that $\mathcal{Y}^{\text{RC}} = \tilde{\mathcal{Y}}^{\text{RC}} + \mathcal{V}^{\text{RC}}$, where \mathcal{V}^{RC} represents the additive noise tensor. Upon closer examination, $\tilde{\mathcal{Y}}^{\text{RC}}$ can be viewed as a slice-wise product between the effective UT-HRIS channel \mathcal{C} and the coded symbol tensor \mathcal{S} , and can be written using the n -mode product notation [57] as $\mathcal{C} = \mathcal{T}_{\Phi} \times_1 \mathbf{I}_{N_c} \times_2 \mathbf{G}^T \times_3 \mathbf{I}_K \in \mathbb{C}^{N_c \times L \times K}$ and $\mathcal{S} = \mathcal{W} \times_1 \mathbf{I}_L \times_2 \mathbf{X}^T \times_3 \mathbf{I}_K \in \mathbb{C}^{L \times T \times K}$, respectively, where $\mathcal{T}_{\Phi} \in \mathbb{C}^{N_c \times N \times K}$ is the sensing phase shift tensor, while $\mathcal{W} \in \mathbb{C}^{L \times R \times K}$ is the coding tensor. Using the K -mode slice contraction operator (1), we have

$$\tilde{\mathcal{Y}}^{\text{RC}} = \mathcal{C} \circledast_2^1 \mathcal{S} = (\mathcal{T}_{\Phi} \times_2 \mathbf{G}^T) \circledast_2^1 (\mathcal{W} \times_2 \mathbf{X}^T), \quad (10)$$

From this perspective, the sensed signal at the HRIS results from a mode-wise contraction of the tensors \mathcal{C} and \mathcal{S} , which

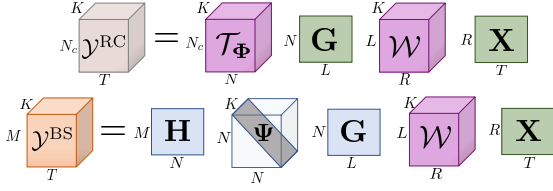


Fig. 3. Tensor structures of the received signals at the HRIS and the BS.

follow Tucker-(1,3) models [58], respectively. We refer to the tensor model in (10) as a *double Tucker* model. Its scalar representation is given by

$$\tilde{y}_{n_c,t,k}^{\text{RC}} = \sum_{n=1}^N \sum_{l=1}^L \sum_{r=1}^R \sqrt{1 - \rho_{n,k}} e^{j\phi_{n_c,n,k}} g_{n,l} w_{l,r,k} x_{r,t}, \quad (11)$$

Likewise, we rewrite (7) as $\mathbf{Y}_{\cdot,k}^{\text{BS}} = \mathbf{H} \Psi_{\cdot,k} \mathbf{G} \mathbf{W}_{\cdot,k} \mathbf{X} + \mathbf{V}_{\cdot,k}^{\text{BS}}$, which matches to the k -th frontal slice of the 3rd-order tensor $\mathcal{Y}^{\text{BS}} \in \mathbb{C}^{M \times T \times K}$. Correspondingly, $\tilde{\mathcal{Y}}^{\text{BS}}$ is the noiseless received signal tensor at the BS, where $\mathcal{Y}^{\text{BS}} = \tilde{\mathcal{Y}}^{\text{BS}} + \mathcal{V}^{\text{BS}}$ and \mathcal{V}^{BS} is the corresponding additive noise tensor. The tensor $\tilde{\mathcal{Y}}^{\text{BS}}$ results from a mode-wise contraction between the *cascaded UT-HRIS-BS channel tensor* \mathcal{T}_{Ω} and the *coded symbol tensor*, where the first follows a PARAFAC model and can be written as $\mathcal{T}_{\Omega} = \mathcal{I}_{3,N} \times_1 \mathbf{H} \times_2 \mathbf{G}^T \times_3 \Psi \in \mathbb{C}^{M \times L \times K}$, where $\Psi = [\psi_1, \dots, \psi_K]^T \in \mathbb{C}^{K \times N}$. Hence, $\tilde{\mathcal{Y}}^{\text{BS}}$ is given by

$$\tilde{\mathcal{Y}}^{\text{BS}} = \mathcal{T}_{\Omega} \circledast_2 \mathcal{S} = (\mathcal{I}_{3,N} \times_1 \mathbf{H} \times_2 \mathbf{G}^T \times_3 \Psi) \circledast_2 (\mathcal{W} \times_2 \mathbf{X}^T). \quad (12)$$

Since the signal tensor received at the BS corresponds to the 3-mode contraction between a PARAFAC and a Tucker-(1,3) models, we refer to (12) as a *PARAFAC-Tucker* model. Its scalar representation is given by

$$\tilde{y}_{m,t,k}^{\text{BS}} = \sum_{n=1}^N \sum_{l=1}^L \sum_{r=1}^R h_{m,n} \sqrt{\rho_{n,k}} e^{j\psi_{n,k}} g_{n,l} w_{l,r,k} x_{r,t}. \quad (13)$$

The mode-wise contraction formalism, applied in (10) and (12), makes it possible to decouple the tensor structures of the transmitted signals and their respective combined/effective channels, revealing their associated (PARAFAC/Tucker) tensor decompositions in a modularized fashion. The received signal tensors at both the HRIS and BS are illustrated in Fig. 3.

Remark 1: If KRSTC is used instead of TSTC, the received signal tensors \mathcal{Y}^{RC} and \mathcal{Y}^{BS} are built the same way, assuming $R = L$. The coded symbol tensor follows a PARAFAC model and is written as $\tilde{\mathcal{S}} = \mathcal{I}_{3,L} \times_1 \mathbf{I}_L \times_2 \mathbf{X}^T \times_3 \mathbf{\Lambda} \in \mathbb{C}^{L \times T \times K}$, where $\mathbf{\Lambda} = [\lambda_1, \dots, \lambda_K]^T \in \mathbb{C}^{K \times L}$. In this case, the received signal tensors are given by $\tilde{\mathcal{Y}}^{\text{RC}} = (\mathcal{T}_{\Phi} \times_2 \mathbf{G}^T) \circledast_2 (\mathcal{I}_{3,L} \times_2 \mathbf{X}^T \times_3 \mathbf{\Lambda})$, and $\tilde{\mathcal{Y}}^{\text{BS}} = (\mathcal{I}_{3,N} \times_1 \mathbf{H} \times_2 \mathbf{G}^T \times_3 \Psi) \circledast_2 (\mathcal{I}_{3,L} \times_2 \mathbf{X}^T \times_3 \mathbf{\Lambda})$, corresponding to *Tucker-PARAFAC* and *double PARAFAC* models, respectively, which are clearly special cases of (10) and (12).

IV. SEMI-BLIND RECEIVERS FOR THE HRIS

In this section, we develop the proposed semi-blind receivers for joint channel and symbol estimation at the HRIS by exploiting the tensor models derived in the previous section. Considering the noisy received signal tensor $\mathcal{Y}^{\text{RC}} = \tilde{\mathcal{Y}}^{\text{RC}} +$

\mathcal{V}^{RC} at the HRIS, the UT-HRIS channel \mathbf{G} and the symbol matrix \mathbf{X} are found by solving the following problem

$$\min_{\mathbf{G}, \mathbf{X}} \left\| \mathcal{Y}^{\text{RC}} - (\mathcal{T}_{\Phi} \times_2 \mathbf{G}^T) \circledast_2 (\mathcal{W} \times_2 \mathbf{X}^T) \right\|_{\text{F}}^2. \quad (14)$$

Starting from this cost function, we formulate two solutions to solve this problem by exploiting the different reshaping of the tensor signal structure. The first one resorts to an iterative alternating linear estimation scheme, while the second delivers closed-form estimates of the channel and symbols.

A. HRIS-BALS receiver

Using the definition (2), and applying $\text{vec}\{\cdot\}$ to the k -th frontal slice of $\tilde{\mathcal{Y}}^{\text{RC}}$, defined in (10), we get $\tilde{\mathbf{y}}_k^{\text{RC}} \doteq \text{vec}\{(\mathcal{C} \circledast_2 \mathcal{S})_{\cdot,k}\} = \mathcal{C}_{\cdot,k} \bullet_1^2 \mathcal{S}_{\cdot,k} = (\mathbf{X}^T \otimes \mathbf{I}_{N_c}) (\mathbf{W}_{\cdot,k}^T \otimes \Phi_{\cdot,k}) \mathbf{g} \in \mathbb{C}^{TN_c \times 1}$, where $\mathbf{g} = \text{vec}\{\mathbf{G}\} \in \mathbb{C}^{LN \times 1}$. We define $\tilde{\mathbf{y}}^{\text{RC}} \doteq [(\tilde{\mathbf{y}}_1^{\text{RC}})^T, \dots, (\tilde{\mathbf{y}}_K^{\text{RC}})^T]^T = \text{vec}\{[\tilde{\mathcal{Y}}^{\text{RC}}]_{(3)}^T\} \in \mathbb{C}^{KT N_c \times 1}$ by stacking $\tilde{\mathbf{y}}_k^{\text{RC}}$ during the K sub-frames, to get

$$\tilde{\mathbf{y}}^{\text{RC}} = (\mathbf{I}_K \otimes \mathbf{X}^T \otimes \mathbf{I}_{N_c}) \mathbf{F}_g \mathbf{g}, \quad (15)$$

where $\mathbf{F}_g \doteq [\mathbf{W}_{\cdot,1} \otimes \Phi_{\cdot,1}^T, \dots, \mathbf{W}_{\cdot,K} \otimes \Phi_{\cdot,K}^T]^T \in \mathbb{C}^{KRN_c \times LN}$ contains the coding structure and the sensing phase shifts, which are known at the HRIS. A least-squares (LS) estimate of the UT-HRIS channel can be found by solving the problem

$$\hat{\mathbf{g}} = \arg \min_{\mathbf{g}} \left\| \tilde{\mathbf{y}}^{\text{RC}} - (\mathbf{I}_K \otimes \mathbf{X}^T \otimes \mathbf{I}_{N_c}) \mathbf{F}_g \mathbf{g} \right\|_{\text{F}}^2, \quad (16)$$

whose analytical solution is given by

$$\hat{\mathbf{G}} = \text{unvec}_{N \times L} \left\{ [(\mathbf{I}_K \otimes \mathbf{X}^T \otimes \mathbf{I}_{N_c}) \mathbf{F}_g]^\dagger \tilde{\mathbf{y}}^{\text{RC}} \right\}, \quad (17)$$

Exploiting $[\tilde{\mathcal{Y}}^{\text{RC}}]_{(2)} = [(\tilde{\mathbf{Y}}_{\cdot,1}^{\text{RC}})^T, \dots, (\tilde{\mathbf{Y}}_{\cdot,K}^{\text{RC}})^T] \in \mathbb{C}^{T \times KN_c}$, corresponding to the 2-mode unfolding of $\tilde{\mathcal{Y}}^{\text{RC}}$, in which $\tilde{\mathbf{Y}}_{\cdot,k}^{\text{RC}} = (\mathcal{C} \circledast_2 \mathcal{S})_{\cdot,k}$ ($k=1, \dots, K$) we have

$$[\tilde{\mathcal{Y}}^{\text{RC}}]_{(2)}^T = \mathbf{F}_x \mathbf{X} \in \mathbb{C}^{KN_c \times T}, \quad (18)$$

where $\mathbf{F}_x \doteq [(\Phi_{\cdot,1} \mathbf{G} \mathbf{W}_{\cdot,1})^T, \dots, (\Phi_{\cdot,K} \mathbf{G} \mathbf{W}_{\cdot,K})^T]^T \in \mathbb{C}^{KN_c \times R}$. The symbol matrix can be found by solving

$$\hat{\mathbf{X}} = \arg \min_{\mathbf{X}} \left\| [\tilde{\mathcal{Y}}^{\text{RC}}]_{(2)}^T - \mathbf{F}_x \mathbf{X} \right\|_{\text{F}}^2, \quad (19)$$

the solution of which is given by

$$\hat{\mathbf{X}} = \mathbf{F}_x^\dagger [\tilde{\mathcal{Y}}^{\text{RC}}]_{(2)}^T. \quad (20)$$

Note that (17) and (20) are jointly used to iteratively estimate the UT-HRIS channel and symbols *via* a bilinear alternating LS (BALS) algorithm, herein referred to as HRIS-BALS receiver. The algorithm consists of estimating \mathbf{G} and \mathbf{X} iteratively, starting from a random initialization until convergence is achieved. As discussed in previous works [52], [24], such a BALS procedure converges after a few iterations and provides unique estimates of the channel and symbol matrices up to trivial scaling ambiguities, as will be discussed later. The HRIS-BALS receiver is summarized in Algorithm 1.

Remark 2: The algebraic steps to derive the BALS receiver at the HRIS for the KRSTC scheme follow (17) and (20) by replacing $\mathbf{W}_{\cdot,k}$ by $\text{diag}\{\lambda_k\}$ and redefining \mathbf{F}_g and \mathbf{F}_x as $\mathbf{F}_g \doteq [\text{diag}\{\lambda_1\} \otimes \Phi_{\cdot,1}^T, \dots, \text{diag}\{\lambda_K\} \otimes \Phi_{\cdot,K}^T]^T \in \mathbb{C}^{KLN_c \times LN}$ and $\mathbf{F}_x \doteq [\text{diag}\{\lambda_1\} \mathbf{G}^T \Phi_{\cdot,1}^T, \dots, \text{diag}\{\lambda_K\} \mathbf{G}^T \Phi_{\cdot,K}^T]^T \in \mathbb{C}^{KN_c \times L}$, where $R = L$ is assumed.

Algorithm 1: HRIS-BALS receiver

1. Set $i = 0$ and initialize $\hat{\mathbf{X}}_{(i=0)}$ randomly;
2. $i = i + 1$;
3. Get $\hat{\mathbf{G}}^{(i)} = \text{unvec}_{N \times L} \{ [(\mathbf{I}_K \otimes \mathbf{X}_{(i-1)}^T \otimes \mathbf{I}_{N_c}) \mathbf{F}_g]^\dagger \mathbf{y}^{\text{RC}} \}$;
4. Get $\hat{\mathbf{X}}^{(i)} = \mathbf{F}_{\mathbf{x}^{(i)}}^\dagger [\mathcal{Y}^{\text{RC}}]_{(2)}^\dagger$;
5. Repeat steps 2-5 until convergence;
6. Remove scaling ambiguities.

Algorithm 2: HRIS-KronF receiver

1. Using (24), find a LS estimate of $\hat{\mathbf{X}}_G$;
2. Construct \mathbf{P}_{xg} by rearranging $\hat{\mathbf{X}}_G$;
3. Compute $[\mathbf{u}_1, \sigma_1, \mathbf{v}_1] \leftarrow \text{truncated-SVD}(\mathbf{P}_{\text{xg}})$;
4. Reconstruct $\hat{\mathbf{G}}$ and $\hat{\mathbf{X}}$:
 $\hat{\mathbf{G}} \leftarrow \text{unvec}_{N \times L} \{ \sqrt{\sigma_1} \mathbf{v}_1^* \}$, $\hat{\mathbf{X}} \leftarrow (\text{unvec}_{T \times R} \{ \sqrt{\sigma_1} \mathbf{u}_1 \})^T$;
5. Remove scaling ambiguities.

B. HRIS-KronF receiver

Define $\tilde{\mathbf{y}}_k^{\text{RC}} \doteq \text{vec}\{(\mathcal{C} \otimes_1^2 \mathcal{S})_{..k}^T\} = (\Phi_{..k} \otimes \mathbf{I}_T) \mathbf{X}_G \mathbf{w}_k \in \mathbb{C}^{N_c T \times 1}$, where $\mathbf{w}_k \doteq \text{vec}\{\mathbf{W}_{..k}^T\} \in \mathbb{C}^{LR \times 1}$ and $\mathbf{X}_G \doteq \mathbf{G} \otimes \mathbf{X}^T \in \mathbb{C}^{NT \times LR}$. Applying $\text{vec}\{\cdot\}$ again, we obtain $\tilde{\mathbf{y}}_k^{\text{RC}} = (\mathbf{w}_k^T \otimes \Phi_{..k} \otimes \mathbf{I}_T) \mathbf{x}_g$, where $\mathbf{x}_g = \text{vec}\{\mathbf{X}_G\} \in \mathbb{C}^{LRNT \times 1}$. Defining $\tilde{\mathbf{y}}^{\text{RC}} \doteq [(\tilde{\mathbf{y}}_1^{\text{RC}})^T, \dots, (\tilde{\mathbf{y}}_K^{\text{RC}})^T]^T = \text{vec}\{[\tilde{\mathcal{Y}}^{\text{RC}}]_{(2)}\}$ collecting the sensed signals during the K sub-frames, we get

$$\tilde{\mathbf{y}}^{\text{RC}} = (\mathbf{F}_{\text{xg}} \otimes \mathbf{I}_T) \mathbf{x}_g \in \mathbb{C}^{KN_c T \times 1}, \quad (21)$$

where $\mathbf{F}_{\text{xg}} \in \mathbb{C}^{KN_c \times LRN}$ is given by

$$\mathbf{F}_{\text{xg}} \doteq [\mathbf{w}_1 \otimes \Phi_{..1}^T, \dots, \mathbf{w}_K \otimes \Phi_{..K}^T]^T. \quad (22)$$

Let us consider the following problem

$$\hat{\mathbf{x}}_g = \arg \min_{\mathbf{x}_g} \|\tilde{\mathbf{y}}^{\text{RC}} - (\mathbf{F}_{\text{xg}} \otimes \mathbf{I}_T) \mathbf{x}_g\|^2, \quad (23)$$

from which we can determine an LS estimate for the matrix \mathbf{X}_G through its corresponding solution

$$\hat{\mathbf{X}}_G = \text{unvec}_{NT \times LR} \{ (\mathbf{F}_{\text{xg}}^\dagger \otimes \mathbf{I}_T) \tilde{\mathbf{y}}^{\text{RC}} \}. \quad (24)$$

Upon obtaining $\hat{\mathbf{X}}_G$, the next step involves finding an estimate of \mathbf{X} and \mathbf{G} from it. To this end, we address the problem

$$\min_{\mathbf{X}, \mathbf{G}} \left\| \hat{\mathbf{X}}_G - \mathbf{G} \otimes \mathbf{X}^T \right\|_{\text{F}}^2, \quad (25)$$

whose solution is found by the so-called Kronecker Factorization (KronF) algorithm [49]. The solution to this problem is found by recasting the problem (25) as a rank-1 matrix approximation problem $\min_{\mathbf{X}, \mathbf{G}} \|\mathbf{P}_{\text{xg}} - \text{vec}\{\mathbf{X}^T\} \text{vec}\{\mathbf{G}\}^T\|_{\text{F}}^2$, where $\mathbf{P}_{\text{xg}} \in \mathbb{C}^{RT \times LN}$ is a matrix rearrangement of the blocks contained in $\hat{\mathbf{X}}_G$ (further details can be found in [49]). From this problem, the estimates of \mathbf{X} and \mathbf{G} are given by the dominant left and right singular vectors of \mathbf{P}_{xg} , respectively. This procedure leads to the HRIS-KronF receiver, whose key steps are summarized in Algorithm 2.

C. HRIS-KRF receiver

For the KRSTC scheme, closed-form estimates of \mathbf{G} and \mathbf{X} are obtained from similar steps analogous to (24) and (25) after minor algebraic modifications. In this case, we have

$$\hat{\mathbf{X}}_G = \text{unvec}_{NT \times L} \{ (\mathbf{F}_{\text{xg}}^\dagger \otimes \mathbf{I}_T) \tilde{\mathbf{y}}^{\text{RC}} \}, \quad (26)$$

Algorithm 3: HRIS-KRF receiver

1. Using (26), find a LS estimate of $\hat{\mathbf{X}}_G$;
2. Given $\mathbf{Q} \leftarrow \hat{\mathbf{X}}_G$, estimate $\hat{\mathbf{G}}$ and $\hat{\mathbf{X}}$:
for $l = 1, \dots, L$
 $\mathbf{Q}_l = \text{unvec}_{T \times N} \{ \mathbf{q}_l \}$
 $[\mathbf{u}_1, \sigma_1, \mathbf{v}_1] \leftarrow \text{truncated-SVD}(\mathbf{Q}_l)$
 $\hat{\mathbf{g}}_l = \sqrt{\sigma_1} \mathbf{v}_1^*$, $\hat{\mathbf{x}}_l = \sqrt{\sigma_1} \mathbf{u}_1$
end;
3. $\hat{\mathbf{G}} \leftarrow [\hat{\mathbf{g}}_1, \dots, \hat{\mathbf{g}}_L]$, $\hat{\mathbf{X}} \leftarrow [\hat{\mathbf{x}}_1, \dots, \hat{\mathbf{x}}_L]^T$;
4. Remove scaling ambiguities.

where $\mathbf{F}_{\text{xg}} \doteq [\boldsymbol{\lambda}_1 \otimes \Phi_{..1}^T, \dots, \boldsymbol{\lambda}_K \otimes \Phi_{..K}^T]^T \in \mathbb{C}^{KN_c \times LN}$. Once $\hat{\mathbf{X}}_G$ is found, we solve the problem $\min_{\mathbf{X}, \mathbf{G}} \|\hat{\mathbf{X}}_G - \mathbf{G} \otimes \mathbf{X}^T\|_{\text{F}}^2$, for which can be solved using the Khatri-Rao Factorization (KRF) algorithm [24], [59]. This algorithm corresponds to solving L rank-1 matrix approximation subproblems, where each subproblem operates on the reshaping of the l -th column of $\hat{\mathbf{X}}_G$ into a rank-1 matrix $\mathbf{Q}_l \in \mathbb{C}^{T \times N}$. The l -th columns of $\hat{\mathbf{X}}^T$ and $\hat{\mathbf{G}}$ are respectively found from the dominant left and right singular vectors of \mathbf{Q}_l , respectively. The HRIS-KRF receiver is summarized in Algorithm 3.

Remark 3: The HRIS does not need to estimate the full information contained in the symbol matrix. It may be of interest to only decode a subset of columns of \mathbf{X} , leaving the remaining subset to be decoded by the BS. As elucidated in Section VIII, \mathbf{X} can be partitioned into user data and control data submatrices during the transmission time structure. For ease of exposition, we consider that HRIS and BS fully estimate the symbol matrix. Note also that even in a scenario where the HRIS does not need to perform data decoding, the proposed semi-blind receivers provide data-aided CE capabilities at the HRIS. In this scenario, data symbols intended for the BS are exploited at the HRIS to estimate the associated channel matrix, as opposed to existing methods, which accomplish this by using only pilot symbols.

V. SEMI-BLIND RECEIVERS FOR THE BS

As for the HRIS, joint symbol and CE can be achieved at the BS by exploiting the tensor structure of the received signal \mathcal{Y}^{BS} as well as the estimated UT-HRIS channel matrix obtained at the HRIS and conveyed *via* the CL. Recall that the BS knows the coding tensor and the reflection phase shifts. We consider the following LS tensor fitting problem

$$\min_{\mathbf{H}, \mathbf{X}} \left\| \tilde{\mathcal{Y}}^{\text{BS}} - \left(\mathcal{I}_{3,N} \times_1 \mathbf{H} \times_2 \hat{\mathbf{G}}^T \times_3 \Psi \right) \otimes_2^1 (\mathcal{W} \times_2 \mathbf{X}^T) \right\|_{\text{F}}^2. \quad (27)$$

In what follows, we exploit the different reshapings of the received tensor \mathcal{Y}^{BS} to derive the corresponding iterative and closed-form semi-blind receivers at the BS.

A. BS-BALS receiver

Concatenating the frontal slices $\tilde{\mathbf{Y}}_{..k}^{\text{BS}} = (\mathcal{T}_\Omega \otimes_1^2 \mathcal{S})_{..k}$ and $\tilde{\mathbf{Y}}_{..k}^{\text{BS}}$ for $k = 1, 2, \dots, K$, we can obtain the 1-mode and 2-mode unfoldings of the received tensor $\tilde{\mathcal{Y}}^{\text{BS}}$, given by $[\tilde{\mathcal{Y}}^{\text{BS}}]_{(1)} = [\tilde{\mathbf{Y}}_{..1}^{\text{BS}}, \dots, \tilde{\mathbf{Y}}_{..K}^{\text{BS}}] \in \mathbb{C}^{M \times KT}$ and $[\tilde{\mathcal{Y}}^{\text{BS}}]_{(2)} = [(\tilde{\mathbf{Y}}_{..1}^{\text{BS}})^T, \dots, (\tilde{\mathbf{Y}}_{..K}^{\text{BS}})^T] \in \mathbb{C}^{T \times KM}$. These unfoldings can be expressed in compact form as

$$[\tilde{\mathcal{Y}}^{\text{BS}}]_{(1)} = \mathbf{H} \mathbf{E}_h (\mathbf{I}_K \otimes \mathbf{X}), \quad (28)$$

$$[\tilde{\mathcal{Y}}^{\text{BS}}]_{(2)}^T = (\mathbf{I}_K \otimes \mathbf{H}) \mathbf{E}_x \mathbf{X}, \quad (29)$$

Algorithm 4: BS-BALS receiver

1. Get $\hat{\mathbf{G}}$ from the feedback control link;
2. Set $i = 0$ and initialize $\hat{\mathbf{X}}_{(i=0)}$ randomly;
3. $i = i + 1$;
4. Get $\hat{\mathbf{H}}_{(i)} = [\mathcal{Y}^{\text{BS}}]_{(1)} [\mathbf{E}_{\text{h}(i-1)} (\mathbf{I}_K \otimes \hat{\mathbf{X}}_{(i-1)})]^\dagger$;
5. Get $\hat{\mathbf{X}}_{(i)} = [(\mathbf{I}_K \otimes \hat{\mathbf{H}}_{(i)}) \mathbf{E}_{\text{x}}]^\dagger [\mathcal{Y}^{\text{BS}}]_{(2)}^\text{T}$;
6. Repeat steps 3-6 until convergence;
7. Remove scaling ambiguities.

where $\mathbf{E}_{\text{h}} \in \mathbb{C}^{N \times KR}$ and $\mathbf{E}_{\text{x}} \in \mathbb{C}^{KN \times R}$ are defined as

$$\begin{aligned} \mathbf{E}_{\text{h}} &\doteq [\text{diag}\{\boldsymbol{\psi}_1\} \hat{\mathbf{G}} \mathbf{W}_{\cdot 1}, \dots, \text{diag}\{\boldsymbol{\psi}_K\} \hat{\mathbf{G}} \mathbf{W}_{\cdot K}], \\ \mathbf{E}_{\text{x}} &\doteq [\mathbf{W}_{\cdot 1}^\text{T} \hat{\mathbf{G}}^\text{T} \text{diag}\{\boldsymbol{\psi}_1\}, \dots, \mathbf{W}_{\cdot K}^\text{T} \hat{\mathbf{G}}^\text{T} \text{diag}\{\boldsymbol{\psi}_K\}]^\text{T}. \end{aligned}$$

respectively. From (28) and (29), the estimation of the HRIS-BS channel \mathbf{H} and the symbol matrix \mathbf{X} can be obtained by solving the following LS problems

$$\hat{\mathbf{H}} = \arg \min_{\mathbf{H}} \left\| [\mathcal{Y}^{\text{BS}}]_{(1)} - \mathbf{H} \mathbf{E}_{\text{h}} (\mathbf{I}_K \otimes \mathbf{X}) \right\|_{\text{F}}^2, \quad (30)$$

$$\hat{\mathbf{X}} = \arg \min_{\mathbf{X}} \left\| [\mathcal{Y}^{\text{BS}}]_{(2)}^\text{T} - (\mathbf{I}_K \otimes \mathbf{H}) \mathbf{E}_{\text{x}} \mathbf{X} \right\|_{\text{F}}^2, \quad (31)$$

the solutions of which are respectively given by

$$\hat{\mathbf{H}} = [\mathcal{Y}^{\text{BS}}]_{(1)} [\mathbf{E}_{\text{h}} (\mathbf{I}_K \otimes \mathbf{X})]^\dagger, \quad (32)$$

$$\hat{\mathbf{X}} = [(\mathbf{I}_K \otimes \mathbf{H}) \mathbf{E}_{\text{x}}]^\dagger [\mathcal{Y}^{\text{BS}}]_{(2)}^\text{T}. \quad (33)$$

Similarly to the HRIS side, the estimate of the HRIS-BS channel and transmitted symbols can be obtained by solving (32) and (33) iteratively using alternating least-squares. This algorithm is referred to as the BS-BALS receiver and is summarized in Algorithm 4.

Remark 4: For the KRSTC scheme, the BS-BALS receiver follows the steps in (32) and (33) by replacing $\mathbf{W}_{\cdot k}$ by $\text{diag}\{\boldsymbol{\lambda}_k\}$ and redefining $\mathbf{E}_{\text{h}} \in \mathbb{C}^{N \times KL}$ and $\mathbf{E}_{\text{x}} \in \mathbb{C}^{KN \times L}$ as $\mathbf{E}_{\text{h}} \doteq [\text{diag}\{\boldsymbol{\psi}_1\} \hat{\mathbf{G}} \text{diag}\{\boldsymbol{\lambda}_1\}, \dots, \text{diag}\{\boldsymbol{\psi}_K\} \hat{\mathbf{G}} \text{diag}\{\boldsymbol{\lambda}_K\}]$ and $\mathbf{E}_{\text{x}} \doteq [\text{diag}\{\boldsymbol{\lambda}_1\} \hat{\mathbf{G}}^\text{T} \text{diag}\{\boldsymbol{\psi}_1\}, \dots, \text{diag}\{\boldsymbol{\lambda}_K\} \hat{\mathbf{G}}^\text{T} \text{diag}\{\boldsymbol{\psi}_K\}]^\text{T}$, where $R = L$ is assumed.

B. BS-KronF receiver

We now derive the expressions for the closed-form estimation of \mathbf{H} and \mathbf{X} at the BS. The procedure is analogous to that discussed on the HRIS side. First, applying $\text{vec}\{\cdot\}$ to the k -th frontal slice of $\tilde{\mathcal{Y}}^{\text{BS}}$, we get $\tilde{\mathbf{y}}_k^{\text{BS}} \doteq \text{vec}\{(\mathcal{T}_\Omega \otimes_2^1 \mathcal{S})_{\cdot k}\} = (\mathbf{X}^\text{T} \otimes \mathbf{H}) (\mathbf{W}_{\cdot k}^\text{T} \otimes \text{diag}\{\boldsymbol{\psi}_k\}) \hat{\mathbf{g}} \in \mathbb{C}^{TM \times 1}$. Stacking column-wise the received signal vectors $\tilde{\mathbf{y}}_k^{\text{BS}}$, for $k = 1, 2, \dots, K$, we obtain the 3-mode unfolding of $\tilde{\mathcal{Y}}^{\text{BS}}$, given by $[\tilde{\mathcal{Y}}^{\text{BS}}]_{(3)} = [\tilde{\mathbf{y}}_1^{\text{BS}}, \dots, \tilde{\mathbf{y}}_K^{\text{BS}}]^\text{T} \in \mathbb{C}^{K \times TM}$. The transposed version of this unfolding can be expressed as

$$[\tilde{\mathcal{Y}}^{\text{BS}}]_{(3)}^\text{T} = (\mathbf{X}^\text{T} \otimes \mathbf{H}) \mathbf{E}_{\text{xh}} (\mathbf{I}_K \otimes \hat{\mathbf{g}}), \quad (34)$$

where $\mathbf{E}_{\text{xh}} \in \mathbb{C}^{RN \times KLN}$ is defined as

$$\mathbf{E}_{\text{xh}} \doteq [\mathbf{W}_{\cdot 1}^\text{T} \otimes \text{diag}\{\boldsymbol{\psi}_1\}, \dots, \mathbf{W}_{\cdot K}^\text{T} \otimes \text{diag}\{\boldsymbol{\psi}_K\}]. \quad (35)$$

Defining $\mathbf{X}_{\text{H}} \doteq \mathbf{X}^\text{T} \otimes \mathbf{H} \in \mathbb{C}^{TM \times RN}$, we first find its compound estimate by solving the following LS problem

$$\hat{\mathbf{X}}_{\text{H}} = \arg \min_{\mathbf{X}_{\text{H}}} \left\| [\tilde{\mathcal{Y}}^{\text{BS}}]_{(3)}^\text{T} - \mathbf{X}_{\text{H}} \mathbf{E}_{\text{xh}} (\mathbf{I}_K \otimes \hat{\mathbf{g}}) \right\|_{\text{F}}^2, \quad (36)$$

Algorithm 5: BS-KronF receiver

1. Get $\hat{\mathbf{G}}$ from the feedback control link;
2. Using (37), find an LS estimate of $\hat{\mathbf{X}}_{\text{H}}$;
3. Construct \mathbf{P}_{xh} by rearranging $\hat{\mathbf{X}}_{\text{H}}$;
4. Compute $[\mathbf{u}_1, \sigma_1, \mathbf{v}_1] \leftarrow \text{truncated-SVD}(\mathbf{P}_{\text{xh}})$;
5. Reconstruct $\hat{\mathbf{X}}$ and $\hat{\mathbf{H}}$:
 $\hat{\mathbf{X}} \leftarrow [\text{unvec}_{T \times R}\{\sqrt{\sigma_1} \mathbf{v}_1^*\}]^\text{T}$, $\hat{\mathbf{H}} \leftarrow \text{unvec}_{M \times N}\{\sqrt{\sigma_1} \mathbf{u}_1\}$;
6. Remove scaling ambiguities.

the solution of which is given by

$$\hat{\mathbf{X}}_{\text{H}} = [\mathcal{Y}^{\text{BS}}]_{(3)}^\text{T} [\mathbf{E}_{\text{xh}} (\mathbf{I}_K \otimes \hat{\mathbf{g}})]^\dagger. \quad (37)$$

From the estimate $\hat{\mathbf{X}}_{\text{H}}$, we can jointly find the individual estimates of the \mathbf{X} and \mathbf{H} by solving the problem

$$\min_{\mathbf{X}, \mathbf{H}} \left\| \hat{\mathbf{X}}_{\text{H}} - \mathbf{X}^\text{T} \otimes \mathbf{H} \right\|_{\text{F}}^2, \quad (38)$$

which is solved via the KronF algorithm [49]. In our context, this is accomplished by solving the following rank-1 matrix approximation problem $\min_{\mathbf{X}, \mathbf{H}} \|\mathbf{P}_{\text{xh}} - \text{vec}\{\mathbf{H}\} \text{vec}\{\mathbf{X}^\text{T}\}^\text{T}\|_{\text{F}}^2$, where $\mathbf{P}_{\text{xh}} \in \mathbb{C}^{RT \times LN}$ is obtained by rearranging the matrix blocks of $\hat{\mathbf{X}}_{\text{H}}$ (see [60] for details). The main steps of the BS-KronF receiver are summarized in Algorithm 5.

Remark 5: When the KRSTC scheme is used, the estimation steps can be simplified. Applying the $\text{vec}\{\cdot\}$ operator to (9) and using (5), we obtain $[\tilde{\mathcal{Y}}^{\text{BS}}]_{(3)}^\text{T} = \mathbf{X}_{\text{H}} \text{diag}\{\hat{\mathbf{g}}\} \mathbf{E}_{\text{xh}}$, where $\mathbf{E}_{\text{xh}} \doteq \boldsymbol{\Lambda}^\text{T} \diamond \boldsymbol{\Psi}^\text{T} \in \mathbb{C}^{LN \times K}$ is constructed from the definitions of $\boldsymbol{\Psi}$ and $\boldsymbol{\Lambda}$ (in Section III). This way, we get $\hat{\mathbf{X}}_{\text{H}} = [\mathcal{Y}^{\text{BS}}]_{(3)}^\text{T} (\text{diag}\{\hat{\mathbf{g}}\} \mathbf{E}_{\text{xh}})^\dagger \in \mathbb{C}^{TM \times LN}$. Then, we invoke Algorithm 5 to estimate $\mathbf{X} \in \mathbb{C}^{T \times L}$ and $\mathbf{H} \in \mathbb{C}^{M \times N}$.

Remark 5: It is worth noting that in a scenario where the estimated symbol matrix $\hat{\mathbf{X}}$ is also conveyed to the BS via the CE, the receiver processing simplifies to a simple LS estimation step to estimate $\hat{\mathbf{H}}$. This special case is referred to here simply as ‘‘LS’’. Although this approach will increase the control link load, it serves as a performance reference that will be considered in our numerical evaluations.

VI. IDENTIFIABILITY, UNIQUENESS AND COMPLEXITY

Estimating \mathbf{X} , \mathbf{G} , and \mathbf{H} at the HRIS and BS requires solving a sequence of LS estimation steps that should ensure a unique solution. For the TSTC scheme, this takes into account satisfying the identifiability conditions of (17) and (20) for the iterative receiver BALS, and (24) for the closed-form receiver KronF at the HRIS, which are $KN_c \geq R$, $KTN_c \geq LN$ and $KN_c \geq LRN$, respectively. Similarly, at the BS, we need to ensure the conditions $KM \geq R$ and $KT \geq N$ for BALS, and $K \geq RN$ for KronF, as per (32), (33), and (37). Analogous considerations should be made for the KRSTC scheme. The identifiability conditions required to satisfy each receiver (at both the HRIS and BS) are summarized in Table I for both TSTC and KRSTC schemes, which are presented in terms of the minimum number K of sub-frames necessary to ensure the estimation of the corresponding channel and symbol matrices. Note that for BALS receivers, the conditions necessary to estimate both matrices must be satisfied simultaneously. To address this, simplified conditions meeting this requirement

TABLE I
IDENTIFIABILITY CONDITIONS AND COMPUTATIONAL COMPLEXITIES.

Receiver	Entity	Coding	Condition $K \geq \lceil \cdot \rceil$	Complexity $\mathcal{O}(\cdot)$
BALS	HRIS	TSTC	$(1/N_c)\max\{R, LN/T\}$	$KN_c(R^2 + L^2N^2T)$
KronF	HRIS	TSTC	LRN/N_c	$LRN(LRNKN_c + T)$
BALS	BS	TSTC	$\max\{R/M, N/T\}$	$K(R^2M + N^2T)$
KronF	BS	TSTC	RN	$RN(RNK + TM)$
BALS	HRIS	KRSTC	$(1/N_c)\max\{L, LN/T\}$	$L^2KN_c(1 + N^2T)$
KRF	HRIS	KRSTC	LN/N_c	$LN(LNKN_c + T)$
BALS	BS	KRSTC	$\max\{L/M, N/T\}$	$K(L^2M + N^2T)$
KronF	BS	KRSTC	LN	$LN(LNK + TM)$

are provided in Table I. As the joint symbol and CE can be accomplished iteratively or in closed form, there are four possible combinations of HRIS-BS receiver pairs for each coding scheme (TSTC or KRSTC). In the TSTC scheme, the four receiver pairs are BALS-BALS, BALS-KronF, KronF-BALS, and KronF-KronF. In the KRSTC scheme, we have BALS-BALS, BALS-KronF, KRF-BALS, and KRF-KronF. These terminologies will be used in Section VII, where the numerical results of the different receiver pairs will be evaluated.

Once the conditions outlined in Table I are met, the estimated matrices $\hat{\mathbf{G}}$ and $\hat{\mathbf{X}}$ (at the HRIS) and $\hat{\mathbf{H}}$ and $\hat{\mathbf{X}}$ (at the BS) share scaling ambiguities that mutually compensate each other. At the HRIS side, and assuming the TSTC scheme, such a relationship is $\hat{\mathbf{X}} = \alpha\mathbf{X}$ and $\hat{\mathbf{G}} = (1/\alpha)\mathbf{G}$. On the other hand, for the KRSTC scheme, we have $\hat{\mathbf{X}} = \Delta_x\mathbf{X}$ and $\hat{\mathbf{G}} = \mathbf{G}\Delta_g$, where $\Delta_x, \Delta_g \in \mathbb{C}^{L \times L}$ are diagonal matrices such that $\Delta_x\Delta_g = \mathbf{I}_L$. Hence, for TSTC, the scaling ambiguities can be mitigated simply by sending a single pilot embedded into the transmitted data. A simple choice is to set $\mathbf{X}_{:,1} = 1$. This knowledge allows us to find α to eliminate the scaling ambiguity through normalization. On the other hand, for KRSTC, computing Δ_x implies the knowledge of one column of $\mathbf{X} \in \mathbb{C}^{L \times T}$ in order to eliminate the scaling ambiguities. In this case, the UT can send a pilot embedded in the first symbol period of each data stream. A straightforward option is to consider $\mathbf{X}_{:,1} = [1, \dots, 1]^T$. For both coding schemes, the scaling ambiguities affecting the estimated channel and symbol matrices at the BS are given by $\hat{\mathbf{X}} = \beta\mathbf{X}$ and $\hat{\mathbf{H}} = (1/\beta)\mathbf{H}$, which can also be eliminated using the same procedure discussed for the HRIS side.

As far as computational complexity is concerned, let us first recall the complexity of the matrix inverse. We consider a complexity of $\mathcal{O}(I^2J)$ to calculate the pseudo-inverse of a tall matrix $\mathbf{A} \in \mathbb{C}^{I \times J}$, where $\text{rank}\{\mathbf{A}\} = I$. For the iterative BALS algorithms, the complexity of each iteration is dominated by the two matrix inverses in (17) and (20) (for the HRIS-BALS receiver) and in (32) and (33) (for the BS-BALS receiver). The overall complexity is given by multiplying the complexity of a single iteration by the number of iterations to convergence. Moreover, note that the complexity of computing the truncated-SVD(\mathbf{A}) is assumed to be $\mathcal{O}(IJ\text{rank}\{\mathbf{A}\})$. In the particular case of the KronF algorithms, the complexity is given by that of the LS estimation step in the first stage, given by (24) for the HRIS-KronF receiver and by (37) for the BS-KronF receiver, followed by the complexity associated with computing a rank-1 matrix approximation steps associ-

ated with the Kronecker factorization problems in (25) and (38), respectively. Finally, the KRF algorithm (considered at the HRIS under the KRSTC scheme) involves solving (26) followed by L rank-1 matrix approximation routines. Table I lists the complexity of all receivers discussed in this work, with the complexity of all BALS receivers provided per iteration.

VII. SIMULATION RESULTS

We adopt a distance-dependent path loss (PL) model, given by $\text{PL} = \text{PL}_0(d/d_0)^{-\alpha}$, in which $\text{PL}_0 = -20$ dB is the path loss at the reference distance $d_0 = 1$ m, d is the individual link distance, and α denotes the path loss exponent. We consider $d_u = 30$ m, $d_h = 70$ m, and following [19], we set $\alpha_g = 2.1$ and $\alpha_h = 2.2$ as, respectively, the UT-HRIS and HRIS-BS link distances and path loss exponents. We assume the Rayleigh fading channel model, in which the UT-HRIS and HRIS-BS channels are taken from a zero-mean independent and identically distributed (i.i.d.) complex-valued Gaussian distribution with variances γ and β , respectively, corresponding to the path losses of these links. We generated the noise level according to the transmit SNR (t-SNR) values. To keep analyses simple, we choose the transmit power to be unity, and both HRIS and BS have the same noise power level. Given that the energy coupling level is dictated through meta-atom design, as highlighted in [1], we allocate the same coupling level to all meta-atoms, and we assume the ρ parameter is non-reconfigurable to simplify the assessment. We design the reflecting and sensing phase shifts as well as the coding (for both TSTC and KRSTC) according to Appendix A. The symbol matrix \mathbf{X} is based on a 64-QAM constellation. We evaluate joint symbol and CE accuracies by means of the symbol error rate (SER) and the normalized mean square error (NMSE), respectively. Each result is an average over at least 10^4 independent Monte Carlo runs. Each run considers different realizations of the symbols, channels, and noise. To ensure a fair comparison between the proposed TSTC and KRSTC schemes, we set $R = L$ and dismiss the entire first column of $\hat{\mathbf{X}} \in \mathbb{C}^{R \times T}$ to calculate the SER (not only $\hat{\mathbf{X}}_{:,1}$). Unless otherwise stated, we assume the parameter set $\{M, N, N_c, L, R, T, K\} = \{8, 32, 2, 2, 2, 4, 64\}$.

Firstly, we examine the trade-off between the semi-blind CE accuracy and the ρ parameter, shown in Fig. 4. To inspect symbol estimation at both HRIS and BS, we selected the scenario in which only $\hat{\mathbf{G}}$ is sent *via* the CL, which implies using semi-blind receivers on both sides. We chose the KronF and BALS receivers for the HRIS and BS, respectively. When ρ approaches 0, the HRIS becomes a quasi “only detecting (not reflecting) RIS”, causing low SER values at the HRIS, while at the BS, they approach 1. As ρ increases, the symbol estimation performance is degraded at the HRIS due to the decreased sensing/detection capability. In contrast, the estimation accuracy at the BS side is enhanced as the reflected signal arrives at the BS with greater strength. Likewise, higher values of ρ imply an increase in the NMSE of $\hat{\mathbf{G}}$ while decreasing the NMSE of $\hat{\mathbf{H}}$, as predicted in [19]. Since the CE capability at the HRIS is less affected by path loss in our setup (the HRIS is closer to the UT than the BS), the estimation accuracy for the channel $\hat{\mathbf{G}}$ remains much higher even by

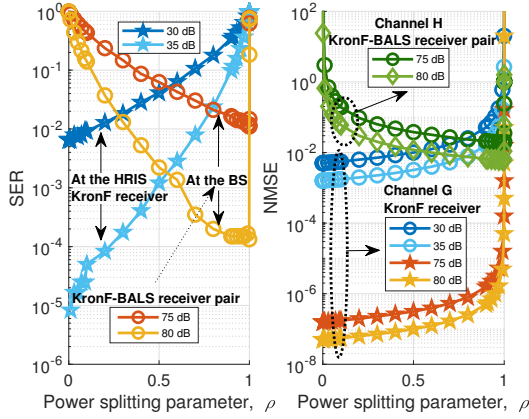


Fig. 4. Behavior of SER vs. ρ , evaluated at both the HRIS and BS, and the corresponding NMSE of the individual channels.

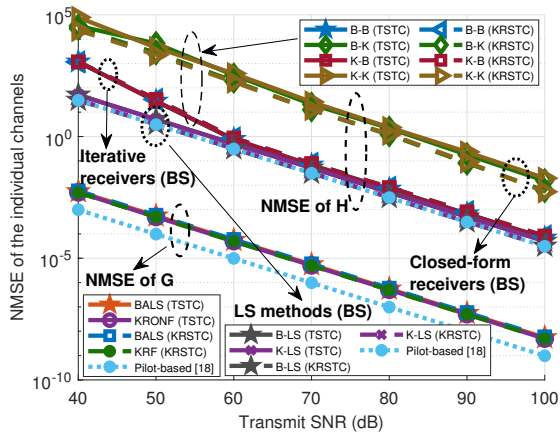


Fig. 5. NMSE of the individual channels vs. transmit SNR (dB).

decreasing the sensing capability (i.e., increasing ρ). However, when ρ approaches 1, and the HRIS behaves closer to a “pure reflecting RIS”, the improvement on the estimates of $\hat{\mathbf{H}}$ at the BS stops, since the accuracy of $\hat{\mathbf{G}}$ becomes compromised. In addition, from the left subfigure of Fig. 4, we can note that for smaller values of ρ , the SER performance at the HRIS is more sensitive to the chosen t-SNR value. The same happens with the SER performance at the BS for higher values of ρ . On the other hand, the right subfigure shows that the channel estimation performances are less sensitive to the variation of the t-SNR compared to the SER ones.

In the next experiments, all the results consider $\rho = 90\%$. Since the BS experiences higher path loss due to the cascaded (UT-HRIS-BS) link, this choice allocates more power to the reflected signal part. Despite the lower power allocated to the sensed signal part, the low path loss associated with the UT-HRIS link still ensures reliable symbol detection and CE at the HRIS. In Fig. 5, we study the NMSE performances at the HRIS and the BS as a function of the t-SNR. We depict the NMSE of the individual channels \mathbf{G} (estimated at the HRIS) and \mathbf{H} (estimated at the BS). On the other hand, Fig. 6 displays the SER results associated with the symbol detection at both HRIS and BS. In both figures, we compare the performances of the proposed semi-blind receiver pairs using TSTC and KRSTC. Let us first start with the performance on the HRIS

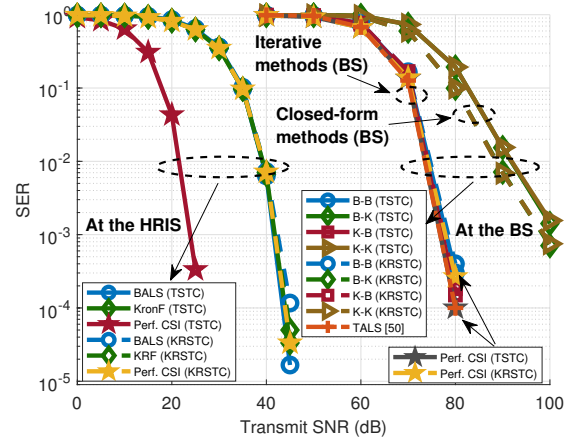


Fig. 6. Symbol error rate vs. transmit SNR (dB).

side. As a reference for comparisons, in Fig. 5, we also plot the performance of the pilot-assisted case based on [19] using the same set of parameters⁶, wherein we apply a simple LS solution to estimate \mathbf{G} at the HRIS and \mathbf{H} at the BS. As shown in Figs. 5 and 6, all semi-blind receivers operating at the HRIS exhibit the same NMSE and SER performances (for both TSTC and KRSTC), with the HRIS offering higher accuracy in symbol and CE compared to the BS due to its positioning. Such results align with those reported in [19] in the CE scope (see Fig. 11 therein). Moreover, the spatial diversity introduced by analog combining at the HRIS also contributes to improved performance. However, from Fig. 5, estimating (additionally) the symbol matrix implies a price to be paid (~ 7 dB) in terms of required t-SNR compared to the baseline pilot-assisted method [19], which is restricted to only estimate the channel \mathbf{G} using the full knowledge of \mathbf{X} . Therefore, we can consider the pilot-assisted case as a lower bound to the proposed semi-blind receivers in terms of CE performance. Furthermore, the semi-blind approach allows the UT to transmit data symbols instead of only pilot sequences within the same time-division structure. Indeed, adding a joint symbol and CE functionality at the HRIS can unlock new potential for RIS-aided wireless communication systems, which will be further discussed in Section VIII. Regarding symbol estimation, Fig. 6 shows that all the receivers performed competitively for both coding schemes, corroborating our numerical results shown previously. These results also highlight that when the HRIS has perfect CSI, TSTC offers higher symbol estimation accuracy than KRSTC due to the tensor coding gain provided by the former scheme. These results represent a remarkable milestone in symbol estimation utilizing the hybrid architecture proposed by [1] using only two RF chains out of $N = 32$ HRIS elements.

Still considering Figs. 5 and 6, let us now focus on the BS performance by considering all possible HRIS-BS receiver pairs/combinations. We use the shorthand labels “B” for BALS and “K” for KronF for presentation convenience. Specifically,

⁶We adapted the signal model of [19] to the single-user case. In this case, we design \mathbf{X} as a truncated discrete Fourier transform (DFT) matrix. Since HRIS optimization is out of the scope of our work, and to keep the fair comparison, we do not leverage the optimization procedure proposed in [19].

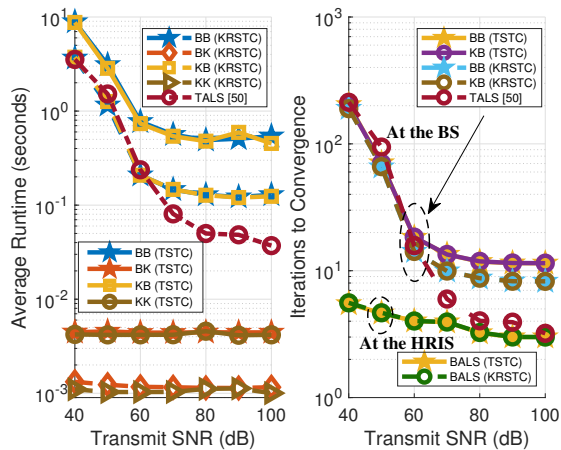


Fig. 7. Average run time (in seconds) for all receiver pairs, and iterations required for convergence of the iterative methods vs. transmit SNR (dB).

on the HRIS side, “K” represents the KronF receiver for the TSTC scheme and the KRF receiver for the KRSTC scheme⁷. Moreover, we use the label “LS” to denote a special (reference) BS receiver that estimates \mathbf{H} assuming the full knowledge of $\hat{\mathbf{X}}$ and $\hat{\mathbf{G}}$ found at the HRIS and conveyed *via* the CL to the BS. To assist us in the discussion, Fig. 7 displays the average run time (in seconds) and the number of iterations required for convergence of the iterative algorithms as a function of the t-SNR for all HRIS-BS receiver pairs. Additionally, Fig. 8 shows the evolution of the computational complexity with respect to the number of HRIS elements. Regarding HRIS-BS CE performance (Fig. 5), all receiver pairs that utilized LS solutions and BALS receivers at the BS performed similarly and demonstrated improved estimation accuracy. Their NMSE curves closely resemble the baseline, particularly KRF-LS and BALS-LS for KRSTC. The accurate estimation obtained at the HRIS effectively narrowed the performance gap at the BS between pilot-based and semi-blind methods, significantly reducing the performance disparities. Note that scenarios in which $\hat{\mathbf{X}}$ and $\hat{\mathbf{G}}$ are conveyed *via* the CL result in solutions with lower computational complexities and less restrictive design requirements, reaching the best results in terms of joint symbol and CE. However, this reference method requires more feedback associated with the conveyance of $\hat{\mathbf{X}}$ estimated at the HRIS, especially when it has larger dimensions. It is worth mentioning that under the same number of UT antennas, the TSTC scheme can allocate more streams than the number L of transmit antennas, which is an interesting setup not possible with the KRSTC scheme. Moreover, the BALS receivers have the distinguishing feature of refining the channel and symbol estimates at each iteration, based only on the estimated $\hat{\mathbf{G}}$ reported by the HRIS. Additionally, the BALS-based receivers can operate under more flexible system setups compared to the closed-form ones. In contrast, their overall complexity depends on the SNR since the number of iterations required for convergence increases for lower SNRs, as indicated in

⁷For example, “B-K (TSTC)” represents the BALS-KronF receiver pair, where BALS is used at the HRIS to estimate the channel $\hat{\mathbf{G}}$ while KronF is used at the BS to estimate \mathbf{H} using $\hat{\mathbf{G}}$ estimated at the HRISs, obtained *via* the CL, and assuming the TSTC scheme.

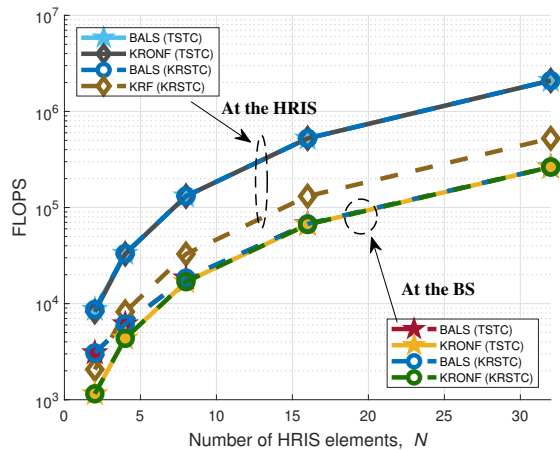


Fig. 8. Number of FLOPs vs. number of HRIS elements.

Fig. 7. On the other hand, when the KronF-based closed-form receivers are used at the BS (Fig. 5), the CE accuracy is clearly affected, revealing a gap with respect to the iterative ones. From Table I, note that $K = 64$ sub-frames are more than enough to meet the identifiability condition of the iterative receivers, while the KronF ones operate tightly at its minimum identifiability boundary ($K = RN$ for TSTC and $K = LN$ for KRSTC). Conversely, KronF performs only a single matrix inverse followed by a rank-1 matrix approximation step, which is much less complex than BALS (for both coding schemes). Hence, its run time is quite low compared to the BALS one, as shown in Fig. 7. It is worth mentioning that although the computational complexity of KronF is lower than that of BALS, it implies more restrictive system setups. In addition, we plot the NMSE of the cascaded channel in Fig. 9, evaluated at the BS by adopting the Khatri-Rao structured matrix $\Theta = \mathbf{G}^T \diamond \mathbf{H} \in \mathbb{C}^{LM \times N}$. We observe that the performance of the cascaded CE follows a similar pattern to those obtained from the estimations of \mathbf{H} . This emphasizes the similarity in performance between two groups of methods regarding the estimation at the BS: one group that employs BALS-based iterative semi-blind receivers (to estimate \mathbf{H} and \mathbf{X}) or estimates only \mathbf{H} (semi-blind and pilot-assisted approaches), and the other group that uses KronF-based semi-blind closed-form receivers and shows a performance drop.

To assess symbol estimation performance at the BS, Fig. 6 depicts the results of all receiver pairs with the TALS semi-blind receiver proposed in [50], which is the state-of-the-art method for semi-blind CE for RIS-assisted communications. In our case, the received signal at the BS using KRSTC differs from that of the PRIS one of [50] only by introducing the factor ρ , causing the HRIS to reflect an impinging wave’s fraction instead of $\rho = 1$. The results show that HRIS-BS receiver pairs executing BALS (for both TSTC and KRSTC) at the BS perform similarly to the PRIS case using TALS. It is essential to highlight that the HRIS absorbs 10% of the incident signal’s energy. This is significant, as symbol estimation remains nearly unaffected compared to the PRIS case when employing iterative receivers. Moreover, it is worth pointing out that the proposed receivers provide a scaling

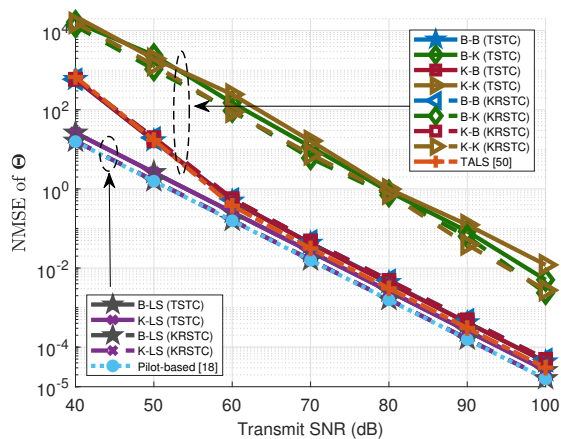


Fig. 9. NMSE of the cascaded channel vs. transmit SNR (dB).

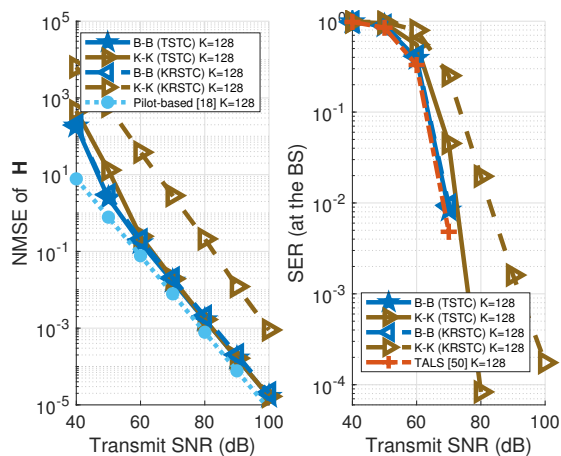


Fig. 10. NMSE of the HRIS-BS channel and SER at the BS evaluated at the BS vs. transmit SNR (dB) for $K = 128$.

ambiguity-free separate CE while decentralizing the CE task, which was previously only performed at the BS. However, one should consider the trade-off between hardware complexity and power consumption. Conversely, the HRIS-BS receiver pairs that apply KronF at the BS confirm the performance drop observed in the previous experiments shown in Fig. 5. These results are also in line with those presented in Fig. 9 for the cascaded CE. Additionally, Fig. 10 shows the NMSE of the HRIS-BS channel and SER at the BS for the K-K and B-B receiver pairs (for both TSTC and KRSTC) as well as for the baseline methods when $K = 128$, i.e., beyond the minimum K required. We can see that KronF, using the TSTC scheme, achieves a significant performance improvement at the BS since the K-K pair approaches the B-B ones and the baseline methods. In contrast, such an increase of K is not sufficient to bring improved performance at the BS when the KRSTC scheme is used. This result emphasizes the gains of the TSTC scheme, as previously mentioned. Note that the benefits provided by the KronF receiver come with the transmission of more sub-frames. This illustrates the interesting tradeoffs offered by the proposed semi-blind HRIS-BS receiver pairs involving performance, complexity, and operating conditions.

VIII. DISCUSSION

In the following, we discuss a few examples of application scenarios and use cases that can potentially benefit from a joint channel and symbol estimation at the HRIS. Relying on direct estimation, *uplink sensing* was considered in [61] in a perceptive mobile network [62] employing joint communication and sensing, which involves the detection of UTs and environmental characteristics between them and remote radio units (RRUs). Therein, symbols are embedded into a sensing matrix, and compressed sensing is applied to estimate delay, Doppler, and angular parameters. The semi-blind approach is suitable to the mentioned joint communication and radar sensing scenario since it dispenses pilot-based training and jointly recovers symbols and channel estimates in a one-way time protocol employing simple receiver algorithms. Furthermore, multiple HRISs can be distributed to serve as decentralized uplink sensing points while alleviating the processing load at the BS. It is worth pointing out that recent works have considered estimating channel parameters at a hybrid RIS. For examples, please refer to [18], [20], [63], [64].

In [65], a multi-antenna UT conveys extra bits to the RIS controller *via* a CL while sending data symbols to the BS *via* the UT-RIS channel during the uplink transmission. Such extra bits are used by the RIS controller to apply an *over-the-air beamforming* technique to improve the transmission. This relies on the prerequisite that there is a CL between the UTs and the RIS. However, maintaining a CL with each active UT can result in a scalability problem since the RIS controller may need to support simultaneous connections with many UTs. This is another suitable application for the proposed semi-blind HRIS processing since control signals can be embedded directly into the data and sent over the UT-RIS link, eliminating or minimizing the dependency on multiple CLs between the HRIS and the UTs. More specifically, the transmitted signals may contain a payload containing both data and control symbols, i.e., the symbol matrix is \mathbf{X} can be partitioned into $\mathbf{X} = [\mathbf{X}_c, \mathbf{X}_d]$, where \mathbf{X}_c contains control symbols to fulfill the mentioned purpose, while \mathbf{X}_d contains data symbols. This way, our semi-blind approach eliminates the need for CLs between UTs and the RIS since \mathbf{X} (or part of it) can be estimated at the HRIS. Otherwise stated, leveraging the information contained in \mathbf{X}_c allows the HRIS to directly decode control signals in a stand-alone fashion.

Another application that can potentially benefit from a joint symbol and channel estimation at the HRIS is vehicular communications. For instance, consider a scenario with multiple roadside RISs placed to serve high-mobility vehicles, as shown in [66]. In [66], assuming that the RIS-BS channel is static, the time-varying UT-RIS channel can be estimated/predicted at the RIS in a decentralized manner, i.e., without the assistance of the BS, minimizing the usage of the CL and avoiding feedback delays and outdated beamforming optimization as a consequence of high UT's mobility. To this, the RIS controller sounds the transmitted pilots by the UT (vehicle) to the BS during the uplink transmission protocol. Bringing this problem to our proposed semi-blind approach, we foresee new use cases allowing UTs to directly share valuable information with their

serving HRIS (and the adjacent ones) by embedding control data such as position, speed, and handover commands into the symbol matrix, which can be decoded at each HRIS and exchanged between in a decentralized way without requiring feedback with their serving BSs. For example, such control data can include speed/position [67], following a similar perspective to that used in *active road safety* [68] applications in vehicular networking.

Finally, we can also envisage a useful scenario where the BS sends control data to (re)configure the HRIS autonomously. In that case, the symbol matrix to be estimated/decoded at the HRIS contains control commands for HRIS configuration purposes or any other relevant network signaling information. This scenario corresponds to an over-the-air HRIS reconfiguration or standalone operation without using the control link.

IX. CONCLUSION

This paper proposed semi-blind joint channel and symbol estimation solutions for hybrid simultaneous reflecting and sensing RIS. Adopting a tensor modeling approach, we revealed the tensor structures of the transmitted signals and the received signals at the HRIS and BS as combinations of PARAFAC and Tucker models, from which novel semi-blind receiver pairs for combined HRIS-BS processing are derived. The proposed tensor-based receivers provide data-aided estimations of the involved channels at both the HRIS and the BS without an *a priori* pilot transmission stage, reducing the symbol decoding delay and improving the data rate. We derived both iterative and closed-form algorithms for joint channel and symbol estimation. We also studied identifiability conditions for guaranteed channel and symbol recovery for each semi-blind receiver pair, revealing the competitive performances of the proposed solutions in comparison with reference methods. Extensive simulation results showcased the performance trends and tradeoffs for the different HRIS-BS receiver pairs. Despite their higher computational complexity, receiver pairs using iterative BALS at the BS offer better estimation accuracy compared to the closed-form (KronF) ones, regardless of the receiver chosen at the HRIS. Our discussion also illuminates the opportunities and use cases arising from empowering HRIS with symbol detection capability. Our numerical results also clarified the impacts of power splitting and tensor coding schemes on channel estimation accuracy and symbol error rates for HRIS-assisted communications. These insights are pivotal for optimizing the system performance in future HRIS deployments. Perspectives include extending the proposed semi-blind receivers to multi-user scenarios and studying alternative tensor-based estimation algorithms.

APPENDIX A DESIGN OF CODING/PHASE-SHIFTS

We jointly design the sensing and reflecting phase shifts by adapting a procedure proposed in [25] while designing the tensor coding separately. We adopt an index vector $\zeta_i^J \triangleq [(i-1)J+1, (i-1)J+2, \dots, iJ] \in \mathbb{R}^{J \times 1}$ for $i = 1, \dots, I$ to denote the i -th block of an IJ -dimensional column vector, in which each block has length of J . Consider a KN_c -dimensional DFT matrix $\mathbf{Z} = [z_1, \dots, z_{KN_c}]$. By

sampling \mathbf{Z} , the 3-mode fibers of \mathcal{T}_Φ and the columns of Ψ are filled by, respectively, $\Phi_{n_c n_c} = z_n(\zeta_{n_c}^K) \in \mathbb{C}^{K \times 1}$ and $\Psi_{\cdot n} = z_{(n-1)N_c+1}(\zeta_1^K) \in \mathbb{C}^{K \times 1}$, for $n_c = 1, \dots, N_c$ and $n = 1, \dots, N$, where the constraint $KN_c \geq N$ is assumed. This yields respectively the following equivalent constructions for \mathcal{T}_Φ and Ψ , defined in Section III:

$$\begin{aligned} [\mathcal{T}_\Phi]_{(3)} &= \begin{bmatrix} z_{1,1} & \cdots & z_{(N_c-1)K+1,1} & \cdots & z_{1,N} & \cdots & z_{(N_c-1)K+1,N} \\ \vdots & \cdots & \vdots & \cdots & \vdots & \cdots & \vdots \\ z_{K,1} & \cdots & z_{N_c K,1} & \cdots & z_{K,N} & \cdots & z_{N_c K,N} \end{bmatrix}, \\ \Psi &= \begin{bmatrix} z_{1,1} & \cdots & z_{1,(N-1)N_c+1} \\ \vdots & \cdots & \vdots \\ z_{K,1} & \cdots & z_{K,(N-1)N_c+1} \end{bmatrix}. \end{aligned}$$

To design the coding tensor \mathcal{W} (TSTC), we first construct the matrix $\Upsilon \in \mathbb{R}^{K \times RL}$ by truncating a K -dimensional Hadamard matrix to its first RL columns, such that $\Upsilon = [\mathbf{W}]_{(3)}$. Then, we get \mathcal{W} by tensorizing Υ or, simply, by doing $\mathbf{W}_{\cdot k} = \text{unvec}_{L \times R} \{\Upsilon_k^T\}$, $k = 1, \dots, K$. For the KRSTC scheme, the coding matrix Λ is designed as a truncated Hadamard matrix, where $K \geq L$. This design can prevent the generalized inverses mentioned in Section VI by replacing them with matrix multiplications through simplified expressions. For KRSTC, this is achieved when $K \geq LN$, and for TSTC, when $K \geq RLN$. Herein, however, we prioritize choosing the minimum number of sub-frames required to ensure joint symbol and CE uniqueness for all semi-blind receivers.

REFERENCES

- [1] G. C. Alexandropoulos, N. Shlezinger, I. Alamzadeh, M. F. Imani, H. Zhang, and Y. C. Eldar, "Hybrid reconfigurable intelligent metasurfaces: Enabling simultaneous tunable reflections and sensing for 6G wireless communications," *IEEE Veh. Technol. Mag.*, vol. 19, no. 1, pp. 75–84, 2024.
- [2] E. Basar *et al.*, "Reconfigurable intelligent surfaces for 6G: Emerging hardware architectures, applications, and open challenges," *IEEE Veh. Technol. Mag.*, vol. 19, no. 3, pp. 27–47, 2024.
- [3] Z. Chen *et al.*, "Reconfigurable-intelligent-surface-assisted B5G/6G wireless communications: Challenges, solution, and future opportunities," *IEEE Commun. Mag.*, vol. 61, no. 1, pp. 16–22, 2023.
- [4] C. Pan *et al.*, "Reconfigurable intelligent surfaces for 6G systems: Principles, applications, and research directions," *IEEE Commun. Mag.*, vol. 59, no. 6, pp. 14–20, 2021.
- [5] C. Huang *et al.*, "Holographic MIMO surfaces for 6G wireless networks: Opportunities, challenges, and trends," *IEEE Wireless Commun.*, vol. 27, no. 5, pp. 118–125, 2020.
- [6] Q. Wu and R. Zhang, "Towards smart and reconfigurable environment: Intelligent reflecting surface aided wireless network," *IEEE Commun. Mag.*, vol. 58, no. 1, pp. 106–112, 2020.
- [7] —, "Beamforming optimization for wireless network aided by intelligent reflecting surface with discrete phase shifts," *IEEE Trans. Commun.*, vol. 68, no. 3, pp. 1838–1851, 2020.
- [8] L. Dong and H.-M. Wang, "Secure MIMO transmission via intelligent reflecting surface," *IEEE Wireless Commun. Lett.*, vol. 9, no. 6, pp. 787–790, 2020.
- [9] S. Alfattani *et al.*, "Aerial platforms with reconfigurable smart surfaces for 5G and beyond," *IEEE Commun. Mag.*, vol. 59, no. 1, pp. 96–102, 2021.
- [10] S. P. Chepuri, N. Shlezinger, F. Liu, G. C. Alexandropoulos, S. Buzzi, and Y. C. Eldar, "Integrated sensing and communications with reconfigurable intelligent surfaces: From signal modeling to processing," *IEEE Signal Process. Mag.*, vol. 40, no. 6, pp. 41–62, 2023.
- [11] Y. Han, W. Tang, X. Li, M. Matthaiou, and S. Jin, "CSI acquisition in RIS-assisted mobile communication systems," *Natl. Sci. Rev.*, vol. 10, no. 8, p. nwad127, 2023.
- [12] M. Di Renzo *et al.*, "Smart radio environments empowered by reconfigurable intelligent surfaces: how it works, state of research, and the road ahead," *IEEE J. Sel. Areas Commun.*, vol. 38, no. 11, pp. 2450–2525, 2020.
- [13] A. L. Swindlehurst, G. Zhou, R. Liu, C. Pan, and M. Li, "Channel estimation with reconfigurable intelligent surfaces — a general framework," *Proc. IEEE*, vol. 110, no. 9, pp. 1312–1338, 2022.
- [14] R. Schroeder, J. He, G. Brante, and M. Juntti, "Two-stage channel estimation for hybrid RIS assisted MIMO systems," *IEEE Trans. Commun.*, vol. 70, no. 7, pp. 4793–4806, 2022.

- [15] Y. Jin, J. Zhang, X. Zhang, H. Xiao, B. Ai, and D. W. K. Ng, "Channel estimation for semi-passive reconfigurable intelligent surfaces with enhanced deep residual networks," *IEEE Trans. Veh. Technol.*, vol. 70, no. 10, pp. 11 083–11 088, 2021.
- [16] J. Zhu, K. Liu, Z. Wan, L. Dai, T. J. Cui, and H. V. Poor, "Sensing RISs: Enabling dimension-independent CSI acquisition for beamforming," *IEEE Trans. Inf. Theory*, vol. 69, no. 6, pp. 3795–3813, 2023.
- [17] S. Yang, W. Lyu, D. Wang, and Z. Zhang, "Separate channel estimation with hybrid RIS-aided multi-user communications," *IEEE Trans. Veh. Technol.*, vol. 72, no. 1, pp. 1318–1324, 2023.
- [18] C. Luo, J. Hu, L. Xiang, and K. Yang, "Reconfigurable intelligent sensing surface aided wireless powered communication networks: A sensing-then-reflecting approach," *IEEE Trans. Commun.*, 2023.
- [19] H. Zhang *et al.*, "Channel estimation with hybrid reconfigurable intelligent metasurfaces," *IEEE Trans. Commun.*, vol. 71, no. 4, pp. 2441–2456, 2023.
- [20] X. Hu, R. Zhang, and C. Zhong, "Semi-passive elements assisted channel estimation for intelligent reflecting surface-aided communications," *IEEE Trans. Wireless Commun.*, vol. 21, no. 2, pp. 1132–1142, 2022.
- [21] Y. Lin, S. Jin, M. Matthaiou, and X. You, "Tensor-based algebraic channel estimation for hybrid IRS-assisted MIMO-OFDM," *IEEE Trans. Wireless Commun.*, vol. 20, no. 6, pp. 3770–3784, 2021.
- [22] S. Liu, Z. Gao, J. Zhang, M. Di Renzo, and M.-S. Alouini, "Deep denoising neural network assisted compressive channel estimation for mmWave intelligent reflecting surfaces," *IEEE Trans. Veh. Technol.*, vol. 69, no. 8, pp. 9223–9228, 2020.
- [23] L. Wei, C. Huang, G. C. Alexandropoulos, C. Yuen, Z. Zhang, and M. Debbah, "Channel estimation for RIS-empowered multi-user MISO wireless communications," *IEEE Trans. Commun.*, vol. 69, no. 6, pp. 4144–4157, 2021.
- [24] G. T. de Araújo, A. L. F. de Almeida, and R. Boyer, "Channel estimation for intelligent reflecting surface assisted MIMO systems: A tensor modeling approach," *IEEE J. Sel. Topics Signal Process.*, vol. 15, no. 3, pp. 789–802, 2021.
- [25] J. Choi and J. H. Cho, "A joint optimization of pilot and phase shifts in uplink channel estimation for hybrid RIS-aided multi-user communication systems," *IEEE Trans. Veh. Technol.*, 2023.
- [26] S. E. Zegrar, L. Afeef, and H. Arslan, "A general framework for RIS-aided mmWave communication networks: Channel estimation and mobile user tracking," *arXiv preprint arXiv:2009.01180*, 2020.
- [27] Q.-U.-A. Nadeem, A. Kammoun, A. Chaaban, M. Debbah, and M.-S. Alouini, "Asymptotic max-min SINR analysis of reconfigurable intelligent surface assisted MISO systems," *IEEE Trans. Wireless Commun.*, vol. 19, no. 12, pp. 7748–7764, 2020.
- [28] R. Li, B. Guo, M. Tao, Y.-F. Liu, and W. Yu, "Joint design of hybrid beamforming and reflection coefficients in RIS-aided mmWave MIMO systems," *IEEE Trans. Commun.*, vol. 70, no. 4, pp. 2404–2416, 2022.
- [29] J. Ye, S. Guo, and M.-S. Alouini, "Joint reflecting and precoding designs for SER minimization in reconfigurable intelligent surfaces assisted MIMO systems," *IEEE Trans. Wireless Commun.*, vol. 19, no. 8, pp. 5561–5574, 2020.
- [30] Y. Sun *et al.*, "Energy-efficient hybrid beamforming for multilayer ris-assisted secure integrated terrestrial-aerial networks," *IEEE Trans. Commun.*, vol. 70, no. 6, pp. 4189–4210, 2022.
- [31] B. Boiadjeva and M. Vu, "Joint multi-user channel estimation for hybrid reconfigurable intelligent surfaces," in *IEEE Int. Conf. Commun.* IEEE, 2023, pp. 877–882.
- [32] S. Yang, W. Lyu, Y. Xiu, Z. Zhang, and C. Yuen, "Active 3D double-RIS-aided multi-user communications: Two-timescale-based separate channel estimation via bayesian learning," *IEEE Trans. Commun.*, 2023.
- [33] C. Hu, L. Dai, S. Han, and X. Wang, "Two-timescale channel estimation for reconfigurable intelligent surface aided wireless communications," *IEEE Trans. Commun.*, vol. 69, no. 11, pp. 7736–7747, 2021.
- [34] X. Chen, J. Shi, Z. Yang, and L. Wu, "Low-complexity channel estimation for intelligent reflecting surface-enhanced massive MIMO," *IEEE Wireless Commun. Lett.*, vol. 10, no. 5, pp. 996–1000, 2021.
- [35] A. Taha, M. Alrabeiah, and A. Alkhateeb, "Enabling large intelligent surfaces with compressive sensing and deep learning," *IEEE Access*, vol. 9, pp. 44 304–44 321, 2021.
- [36] G. C. Alexandropoulos and E. Vlachos, "A hardware architecture for reconfigurable intelligent surfaces with minimal active elements for explicit channel estimation," in *Proc. IEEE Int. Conf. Acoust. Speech Signal Process.* IEEE, 2020, pp. 9175–9179.
- [37] N. Shlezinger, G. C. Alexandropoulos, M. F. Imani, Y. C. Eldar, and D. R. Smith, "Dynamic metasurface antennas for 6G extreme massive MIMO communications," *IEEE Wireless Commun.*, vol. 28, no. 2, pp. 106–113, 2021.
- [38] I. Alamzadeh, G. C. Alexandropoulos, N. Shlezinger, and M. F. Imani, "A reconfigurable intelligent surface with integrated sensing capability," *Sci. Rep.*, vol. 11, no. 1, p. 20737, 2021.
- [39] A. L. F. de Almeida, G. Favier, and J. C. M. Mota, "PARAFAC-based unified tensor modeling for wireless communication systems with application to blind multiuser equalization," *Signal Process.*, vol. 87, no. 2, pp. 337–351, 2007.
- [40] A. L. F. de Almeida, "Tensor modeling and signal processing for wireless communication systems," Ph.D. dissertation, Université de Nice-Sophia Antipolis, 11 2007.
- [41] N. D. Sidiropoulos, G. B. Giannakis, and R. Bro, "Blind PARAFAC receivers for DS-CDMA systems," *IEEE Trans. Signal Process.*, vol. 48, no. 3, pp. 810–823, 2000.
- [42] G. Favier, M. N. da Costa, A. L. F. de Almeida, and J. M. T. Romano, "Tensor space-time (TST) coding for MIMO wireless communication systems," *Signal Process.*, vol. 92, no. 4, pp. 1079–1092, 2012.
- [43] G. Favier and A. L. F. de Almeida, "Tensor space-time-frequency coding with semi-blind receivers for MIMO wireless communication systems," *IEEE Trans. Signal Process.*, vol. 62, no. 22, pp. 5987–6002, 2014.
- [44] H. Chen, F. Ahmad, S. Vorobyov, and F. Porikli, "Tensor decompositions in wireless communications and MIMO radar," *IEEE J. Sel. Topics Signal Process.*, vol. 15, no. 3, pp. 438–453, 2021.
- [45] S. Miron *et al.*, "Tensor methods for multisensor signal processing," *IET Signal Process.*, vol. 14, no. 10, pp. 693–709, 2020.
- [46] N. D. Sidiropoulos, L. De Lathauwer, X. Fu, K. Huang, E. E. Papalexakis, and C. Faloutsos, "Tensor decomposition for signal processing and machine learning," *IEEE Trans. Signal Process.*, vol. 65, no. 13, pp. 3551–3582, 2017.
- [47] A. L. F. de Almeida, G. Favier, J. P. da Costa, and J. C. M. Mota, "Overview of tensor decompositions with applications to communications," in *Signals and Images: Adv. Results in Speech, Estimation, Compression, Recognition, Filtering, and Processing*. CRC-Press, 1 2016, no. Chapter 12, pp. 325–356.
- [48] K. Ardah, S. Gherekhloo, A. L. F. de Almeida, and M. Haardt, "TRICE: A channel estimation framework for RIS-aided millimeter-wave MIMO systems," *IEEE Signal Process. Lett.*, vol. 28, pp. 513–517, 2021.
- [49] G. T. de Araújo, P. R. B. Gomes, A. L. F. de Almeida, G. Fodor, and B. Makkı, "Semi-blind joint channel and symbol estimation in IRS-assisted multiuser MIMO networks," *IEEE Wireless Commun. Lett.*, vol. 11, no. 7, pp. 1553–1557, 2022.
- [50] G. T. de Araújo, A. L. F. de Almeida, R. Boyer, and G. Fodor, "Semi-blind joint channel and symbol estimation for IRS-assisted MIMO systems," *IEEE Trans. Signal Process.*, vol. 71, pp. 1184–1199, 2023.
- [51] P. R. B. Gomes, G. T. de Araújo, B. Sokal, A. L. F. de Almeida, B. Makkı, and G. Fodor, "Channel estimation in RIS-assisted MIMO systems operating under imperfections," *IEEE Trans. Veh. Technol.*, 2023.
- [52] P. Comon, X. Luciani, and A. L. F. de Almeida, "Tensor decompositions, alternating least squares and other tales," *J. Chemom.*, vol. 23, no. 7–8, pp. 393–405, 2009.
- [53] S. Gherekhloo, K. Ardah, A. L. F. de Almeida, and M. Haardt, "An efficient channel training protocol for channel estimation in double RIS-aided MIMO systems," in *2024 32nd European Signal Processing Conference (EUSIPCO)*, 2024, pp. 2067–2071.
- [54] R. A. Harshman and M. E. Lundy, "Uniqueness proof for a family of models sharing features of Tucker's three-mode factor analysis and PARAFAC/CANDECOMP," *Psychometrika*, vol. 61, pp. 133–154, 1996.
- [55] A. L. F. de Almeida, G. Favier, and J. C. M. Mota, "Space-time spreading-multiplexing for MIMO wireless communication systems using the PARATUCK-2 tensor model," *Signal Process.*, vol. 89, no. 11, pp. 2103–2116, 2009.
- [56] N. Sidiropoulos and R. Budampati, "Khatri-Rao space-time codes," *IEEE Trans. Signal Process.*, vol. 50, no. 10, pp. 2396–2407, 2002.
- [57] T. G. Kolda and B. W. Bader, "Tensor decompositions and applications," *SIAM review*, vol. 51, no. 3, pp. 455–500, 2009.
- [58] G. Favier and A. L. F. de Almeida, "Overview of constrained PARAFAC models," *EURASIP Journal of Advances in Signal Processing*, vol. 2014, no. 142, pp. 1–25, Sep. 2014.
- [59] A. Y. Kibangou and G. Favier, "Non-iterative solution for PARAFAC with a toeplitz matrix factor," in *Proc. EUSIPCO*, 8 2009, pp. 691–695.
- [60] C. F. Loan, "The ubiquitous Kronecker product," *Journal of Computational and Applied Mathematics*, vol. 123, no. 1, pp. 85–100, 2000.
- [61] M. L. Rahman, J. A. Zhang, X. Huang, Y. J. Guo, and R. W. Heath, "Framework for a perceptive mobile network using joint communication and radar sensing," *IEEE Trans. Aerosp. Electron. Syst.*, vol. 56, no. 3, pp. 1926–1941, 2019.
- [62] A. Zhang, M. L. Rahman, X. Huang, Y. J. Guo, S. Chen, and R. W. Heath, "Perceptive mobile networks: Cellular networks with radio vision via joint communication and radar sensing," *IEEE Veh. Technol. Mag.*, vol. 16, no. 2, pp. 20–30, 2020.
- [63] G. C. Alexandropoulos, I. Vinieratou, and H. Wymeersch, "Localization via multiple reconfigurable intelligent surfaces equipped with single receive RF chains," *IEEE Wireless Commun. Lett.*, vol. 11, no. 5, pp. 1072–1076, 2022.
- [64] X. Shao, C. You, W. Ma, X. Chen, and R. Zhang, "Target sensing with intelligent reflecting surface: Architecture and performance," *IEEE J. Sel. Areas Commun.*, vol. 40, no. 7, pp. 2070–2084, 2022.
- [65] Z. Yigit, E. Basar, and I. Altunbas, "Over-the-air beamforming with reconfigurable intelligent surfaces," *Front. Comms. Net.*, vol. 3, p. 1016270, 2022.
- [66] Z. Huang, B. Zheng, and R. Zhang, "Roadside IRS-aided vehicular communication: Efficient channel estimation and low-complexity beamforming design," *IEEE Trans. Wireless Commun.*, 2023.
- [67] M. Ahmed *et al.*, "Vehicular communication network enabled CAV data offloading: A review," *IEEE Trans. Intell. Transp. Syst.*, 2023.
- [68] G. Karagiannis *et al.*, "Vehicular networking: A survey and tutorial on requirements, architectures, challenges, standards and solutions," *IEEE Commun. Surveys Tuts.*, vol. 13, no. 4, pp. 584–616, 2011.